Spring 1973

Geology of the Older Precambrian Rocks in the Vicinity of Clear Creek and Zoroaster Canyon, Grand Canyon, Arizona

William S. Lingley Jr.
Western Washington University, lingleyl@comcast.net

GEOLOGY OF THE OLDER PRECAMBRIAN ROCKS IN THE VICINITY OF CLEAR CREEK AND ZOROASTER CANYON, GRAND CANYON, ARIZONA

A Thesis

Presented to

The Faculty of

Western Washington State College

In Partial Fulfillment

Of the Requirements for the Degree

Master of Science

---

by

William S. Lingley

April 1973

MASTER'S THESIS

William S. Lingley, Jr.
February 20, 2018
bill@lesliegeo.com

GEOLOGY OF THE OLDER PRECAMBRIAN ROCKS IN THE VICINITY OF CLEAR CREEK AND ZOROASTER CANYON, GRAND CANYON, ARIZONA

by

William S. Lingley

Accepted in Partial Completion

of the Requirements for the Degree

Master of Science

Dean of Graduate School

Advisory Committee

Chairman

TABLE OF CONTENTS

	Page
INTRODUCTION	1
General Description	1
Previous Research	3
Statement of the Problem Studied	4
Method of Study	4
Acknowledgements	5
THE VISHNU SCHIST	7
General Description	7
Micaceous Schists	8
Biotite	8
Garnet	9
Staurolite	10
Chlorite	10
Sillimanite	19
Other Minerals	19
Amphibolite	21
Meta-Calcsilicates	26
Metamorphism and Metamorphic Grade	26
THE ZOROASTER GNEISS	34
The Vishnu Schist-Zoroaster Gneiss Contact	39
Origin and Emplacement of the Zoroaster Gneiss	42
PEGMATITE AND APLITE	44
STRUCTURES	49
Lithologic Layering	49
Schistosity	49
Lineation	54
Microfolding	54

	Page
Mesoscopic Folding	57
Macroscopic Folding	68
Interpretation of Macroscopic Structures	70
TIME RELATIONSHIPS OF GEOLOGIC EVENTS	71
REFERENCED CITED	73
APPENDIX A: MINERAL ASSEMBLAGES OBSERVED IN THIN SECTION	76

ILLUSTRATIONS

Figure		Page
1.	Index map showing the present study area	2
2.	Map of the Clear Creek-Zoroaster Canyon area showing sample locations	11
3.	Helicitic biotite from sample 46-184	12
4.	Photomicrograph of sample 46-182 showing two foliations	13
5.	Garnet from sample 46-184	14
6.	Relationship of garnet, staurolite, biotite, and sillimanite in sample 46-169	16
7.	Porphyroblastic staurolite from sample 46-176	17
8.	Over-printed chlorite from sample 46-V14	18
9.	View showing the south side of the Inner Gorge of the Colorado R. from mile 85.1 to 85.8	23
10.	Light colored pegmatite and aplite intrusions in darker amphibolite at the east side of Cremation Creek canyon	24
11.	Interpretation of phase relations of sillimanite zone pelitic schists from Clear Creek	32
12.	Zoroaster Gneiss cut by a typical pegmatite dike from upper Zoroaster Canyon	36
13.	Modal analyses of Zoroaster Gneiss, aplite and late granitic rocks	38
14.	View looking north to the Vishnu Schist-Zoroaster Gneiss contact in lower Zoroaster Canyon	41
15.	Some relationships between gneiss, pegmatite, aplite, and quartz in dikes and sills from the Zoroaster Monadnock and Cremation Creek	47
16.	Pegmatite dike in amphibolite from Cremation Creek	48
17.	A map of the attitudes of S_1	51
18.	Equal-area, lower hemisphere projection of 112 poles to foliation in Zoroaster Canyon and the Clear Creek area	52

Figure		Page
19.	View looking northeast into Clear Creek canyon showing vertically oriented schistosity and lithologic layering	53
20.	Boudinage in quartzo-feldspathic veins from lower Clear Creek canyon	55
21.	Photomicrograph of non-penetrative strain-slip cleavage from sample 46-V11	56
22.	Fold with axial plane schistosity (F_1) from Clear Creek	59
23.	Equal-area, lower hemisphere projection of 39 fold axes from the vicinity of Clear Creek	60
24.	Equal-area, lower hemisphere projection of 23 fold axes of concentric folds from Bright Angel Canyon	61
25.	The distribution of some F_2 folds	62
26.	Similar style F_2 fold from Clear Creek	63
27.	F_2 fold showing both concentric and similar styles from Clear Creek	64
28.	Relationship of F_2 and F_4 folds in Clear Creek	65
29.	The relationship between F_2 and F_3 folds	66
30.	Intrafoliation folds and boudinage in quartzo-feldspathic veins from lower Clear Creek canyon	67
31.	Equal-area, lower hemisphere projection of 100 poles to foliation taken west of Zoroaster Canyon	69
32.	Inferred chronologic scheme for the emplacement of rock units, metamorphism, and deformation	72

LIST OF TABLES

Table		Page
1.	Microprobe analyses data for individual minerals from sample 46-183 and 46-184	15
2.	Distribution coefficients for Mg/Mg+Fe in coexisting biotite and garnet from sample 46-184	33
3.	Modal analyses data	40

INTRODUCTION

General Description

The Clear Creek-Zoroaster Canyon area is located in the east-central section of the Bright Angel Quadrangle (Maxson, 1968) roughly seven miles east northeast of Grand Canyon Village, Arizona. The boundaries of the present study area are shown in Figure 1. The study area extends from Mile 83.7 to Mile 86 on the Colorado River below Lee's Ferry, Arizona.

Older Precambrian rocks are exposed along the Inner Gorge of the Colorado River. They also crop out at Zoroaster Canyon, Clear Creek, and Cremation Creek. There are over 450 m of vertical exposure. Many outcrops are inaccessible due to steepness of the canyon walls. The clarity of these exposures is extremely good.

The Older Precambrian rocks exposed within the study area are (1) the Vishnu Schist and associated amphibolites, (2) the Zoroaster Granite, and (3) the late, granitic pegmatites and aplites. All of these rocks show complex inter-relationships, and they are intensely deformed.

In upper Clear Creek the Older Precambrian rocks are unconformably overlain by the younger Precambrian, Grand Canyon Series. The Grand Canyon Series is composed of limestones, shales, and quartzites (Maxson, 1967). Throughout the rest of the study area the older Precambrian rocks show an angular unconformity with the overlying Paleozoic sediments. A summary of Grand Canyon stratigraphy is given by Maxson (1968).

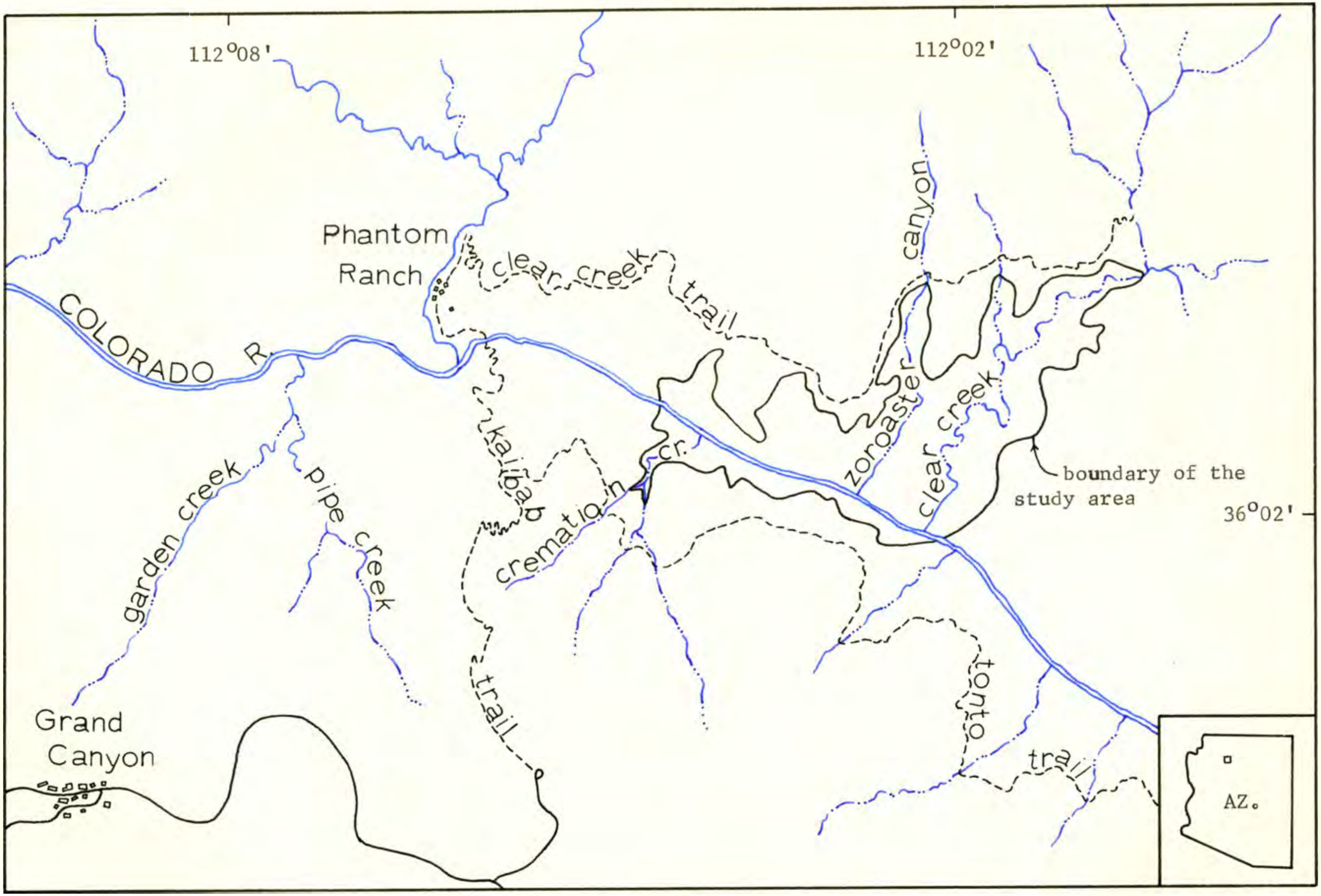

Figure 1. Index map showing the present study area.

Previous Research

Previous to the study reported here there has been no detailed research on the older Precambrian rocks of the Clear Creek-Zoroaster Canyon area. However, several regional studies in the Grand Canyon have dealt with rocks of this age.

Walcott (1894) recognized the Vishnu Schist as the Pre-Unkar Group, bedded metasedimentary rocks. Noble and Hunter (1916) did reconnaissance field work and petrography of samples collected throughout the canyon. They included a few samples from the south side of the Colorado River within the present study area. They noted the late, plastic deformation within the gneiss; the intrusive nature of the pegmatites; and the stock of late granitic rock within the gneiss, west of Zoroaster Canyon.

More extensive studies of these rocks including structural interpretation, petrology, and chemical analyses were done by Campbell and Maxson (1933-1936). They found good evidence for the sedimentary origin of the Vishnu Schist; inferred the presence of macroscopic folds with horizontal axes; and suggested a replacement origin of much of the granitic rock. Maxson (1968) separated the amphibolites into an additional formation, the Brahma Schist. Much of the work of Maxson and Campbell is summarized on Maxson's map (1968).

Ragan and Sheridan (1970) stated that formation status for the amphibolites is unwarranted because amphibolite is thoroughly intermixed with the metasedimentary rock and because the relative ages suggested by Maxson are based on an erroneous structural interpretation. The name Brahma Schist will not be used in this report. Ragan and Sheridan also reported vertical lineations; boudinage which indicates NW-SE shortening of 50% or more; and an inferred, obscure, earlier episode of folding.

Boyce (1972) suggested seven major structural episodes in his detailed study of the Bright Angel Canyon. This canyon is only three miles west of the present study area. Structures such as the NE trending schistosity and the concentric and cyclindrical folding noted by Boyce have been observed in the present study area. Similar conclusions about the mesoscopic folding scheme were reached independently by Boyce and the present writer. His chemical analyses indicate a sediment of greywacke composition for the Vishnu Schist parent. He suggests that the zoning in the pegmatites may be due to hydrothermal enrichment after intrusion.

Pasteels and Silver (1965) have dated zircons from the Zoroaster Gneiss and pegmatites from the Kaibab Trail with the U-Pb method. Their age interpretation for these rocks is 1725 ± 15 myrs. and 1695 ± 15 myrs. respectively.

Statement of the Problem Studied

Although the Clear Creek-Zoroaster Canyon area displays an excellent older Precambrian section, the history of these rocks is poorly understood. This study was undertaken to delineate the structural and metamorphic history of these rocks.

Method of Study

The field studies were carried out in March, April, and May of 1971. Particular attention was paid to the relationships between the various rock units. Two hundred and nine samples were collected to give a volumetrically representative suite and to show the range of lithologic variation.

Thin sections were cut from 110 of these samples. Modal analyses of granitic rock slabs were made using the technique of Chayes (1956). A grid with 100 dots per square centimeter was used for the point counts and a minimum of 1300 counts were made per slab. The staining method of Laniz et al. (1964) proved best for staining plagioclase. Potash feldspar was stained with sodium cobaltinitrite using the method of Bailey and Stevens (1960). Ubiquitous granophyric textures in these rocks made staining difficult. Soaking the slabs in paraffin or acrylic spray, as suggested by Bailey and Stevens, proved useless in improving the adherence of the stain.

The chemical analyses of individual minerals were made using the electron microprobe at the University of Washington. The method used is given in Brown (1967).

Acknowledgements

The writer wishes to convey particular gratitude to Dr. E.H. Brown who served as chairman of the advisory committee. Much of the credit for this study is due to Dr. Brown whose patient instruction and helpful criticism, not only of this report, but over the past several years has made geologic research the primary interest of the writer. Dr. Brown also supplied the chemical analyses of individual minerals used here.

Thanks are given to Dr. R.S. Babcock for serving on the advisory committee, for contributions to this manuscript, and helpful suggestions in many areas of research. Appreciation is extended to Dr. R.C. Ellis for his critical reading of the manuscript and for serving on the advisory committee.

Dr. Brown and Dr. Babcock are thanked for the financial support given this study from their National Science Foundation Grant (GA-31232).

Dr. Ada Swineford was particularly helpful during the early stages of the writing of this report while the advisory committee was absent. The Museum of Northern Arizona contributed materially in the form of a research grant to finance this study, and by the use of their facilities in Flagstaff, Arizona. Special thanks is extended to Mr. Wm. Breed, Curator of Geology at the museum, for his help. The writer also wishes to thank Dr. D.A. Rahm for help with structural interpretation, and Mr. Larry Stavert for petrographic assistance.

During the field work Ms. Patricia Whitcomb's assistance was greatly appreciated.

THE VISHNU SCHIST

General Description

The Vishnu Schist was named by Walcott (1894) and defined as the metasedimentary rocks underlying the Unkar Group. Maxson and Campbell (1933-1935) state that the parent sediments were sandy clays, quartz sands, ferruginous sands, and calcareous sediments. The sedimentary origin of the Vishnu Schist is supported by intercalation on a scale of a few centimeters, and features which are thought to be relict marine cross-bedding and ripple marks (Maxson and Campbell, 1933). The uniform, predominantly sandy clay, sediments are thought to have accumulated in a shallow subsiding geosyncline. The total thickness of the Vishnu Schist is at least 8,500 meters. The thickness may be as great as 18,000 meters since there is considerable repetition of the section (Maxson and Campbell, 1935).

The absolute age of the Vishnu Schist must exceed 1,725 million years, the age of the Zoroaster Gneiss which intrudes it (Pasteels and Silver, 1965).

Exposures of Vishnu Schist in the study area extend from Zoroaster Canyon to 0.5 kilometers east of Clear Creek canyon. The schist displays a pervasive, vertical, northeast striking schistosity.

The major lithologies observed include calcsilicate rocks, impure quartzites, mafic schists, amphibolites and numerous varieties of micaceous schists. Small exposures of chlorite-garnet schist with intensely deformed quartz and potash feldspar veins crop out in upper Clear Creek. Chlorite-garnet-biotite schist also crops out at the contact with the Zoroaster Granite in Zoroaster Canyon. The Vishnu Schist is intruded by a few tourmaline-bearing pegmatite sills in lower Clear Creek.

Micaceous Schists

Mineral assemblages commonly observed in thin sections of micaceous schists are:

biotite-muscovite-chlorite-plagioclase-quartz-
±garnet±staurolite±fibrous sillimanite

Opaques, apatite, tourmaline, and zircon are common accessory minerals. Sample locations are shown in Figure 2 and the complete mineralogy of all micaceous schist samples is given in Appendix A.

There is considerable evidence of poly-metamorphism in these rocks. Euhedral biotite and muscovite appear as cross-micas which cut the schistosity at random angles. Poikiloblastic staurolite and biotite commonly over-print the schistosity. Felts of fibrous sillimanite are present in a few thin sections. Retrograde metamorphism is suggested by patches of chlorite which over-print the schistosity and replace garnets. Chlorite is often associated with the highest grade assemblages in the study area and a chlorite-garnet-biotite rock is in contact with Zoroaster gneiss.

Biotite

Biotite occurs as plates parallel to the schistosity and as large (to 5 mm) porphyroblastic cross-micas. Syntectonic biotites constitute as much as 25 percent of the volume of some samples. Post-tectonic biotite porphyroblasts display helicitic texture where numerous inclusions of quartz, apatite and zircon form sinuous trails (Figure 3). Biotites in sample 46-182 delineate two generations of deformation. The syntectonic biotites form an initial schistosity (S_1) which is cut by a secondary foliation (S_2) formed of post-tectonic biotites (Figure 4). Both foliations are over-printed by randomly oriented biotite porphyroblasts. Fine lamellae of hematite stain the mica blood-red in hand specimen. Chlorite pseudomorphs after biotite are common, though the alteration is seldom complete.

Garnet

Microprobe analysis of a garnet from sample 46-184 gives compositions ranging from 78 to 86 weight percent almandine. The remainder is probably all pyrope and grossularite, however, no manganese analyses were performed. These garnets have outlines which range from subhedral to extremely corroded.

Optical zoning is absent in most samples, but strong chemical zoning of FeO, MgO, and CaO is present. Chemical data from a microprobe traverse of sample 46-184 is given in Table 1. The location of the data points is shown in Figure 5. The core of this garnet is depleted in FeO and MgO while the rim shows marked enrichment in these oxides. Two models have been proposed to explain this zoning pattern: Hollister (1966) hypothesized that most of the MnO present in the minerals surrounding a garnet is consumed by the garnet during its nucleation and early growth. Since the surrounding minerals are rapidly depleted in MnO the rim of the newly formed garnet will be relatively enriched in FeO and MgO. Atherton (1968) and Stuart (1962) suggest that MgO and FeO increase in garnets as a response to increasing grade of metamorphism. In rocks with little MnO in their bulk composition, or with sufficient phases to make the garnets compositionally invariant at constant grade, this is probably the zoning mechanism (Brown, 1969). There are a sufficient number of phases in sample 46-184 so that the enrichment in FeO and MgO probably indicates increasing grade of metamorphism as the garnet grew.

Several of the garnets have straight inclusion trails composed of apatite, tourmaline, opaques, and quartz which cut the foliation at a large angle (see Figure 5). Garnets with this texture are interpreted as early syntectonic or pretectonic relicts (Spry, 1969). Syntectonic, sigmoidal garnets were observed in sample 46-V8. All garnets are porphyroblastic with the foliation bent around them. Some corroded garnets occupy only a small amount of the space they formerly filled. The space vacated by the garnet is filled with quartz, biotite with zircon inclusions, staurolite, and fibrous sillimanite (Figure 6). This texture suggests prograde reactions where garnet is a reactant.

Staurolite

Staurolite appears as porphyroblasts up to 3 cm in length. Commonly these are poikiloblastic with numerous quartz inclusions. Inclusions make up 50 percent of the volume of some staurolites. Staurolite grain boundaries are sharp and well defined; they show no evidence of reaction. In many samples, staurolite porphyroblasts grow at large angles to the foliation. Some of these porphyroblasts appear to forcibly shoulder aside the foliation (Figure 7).

Chlorite

Chlorite has two habits in the micaceous schists: as pseudomorphs after biotite or garnet, and as fresh appearing patches which overprint the foliation (Figure 8). The over-printed variety have sharp grain boundaries and cut the foliation at random angles. Their interference colors are strong shades of blue-violet which indicates an iron-rich composition (Troger, 1959). The over-printed variety has a much stronger green color than the pseudomorphing variety.

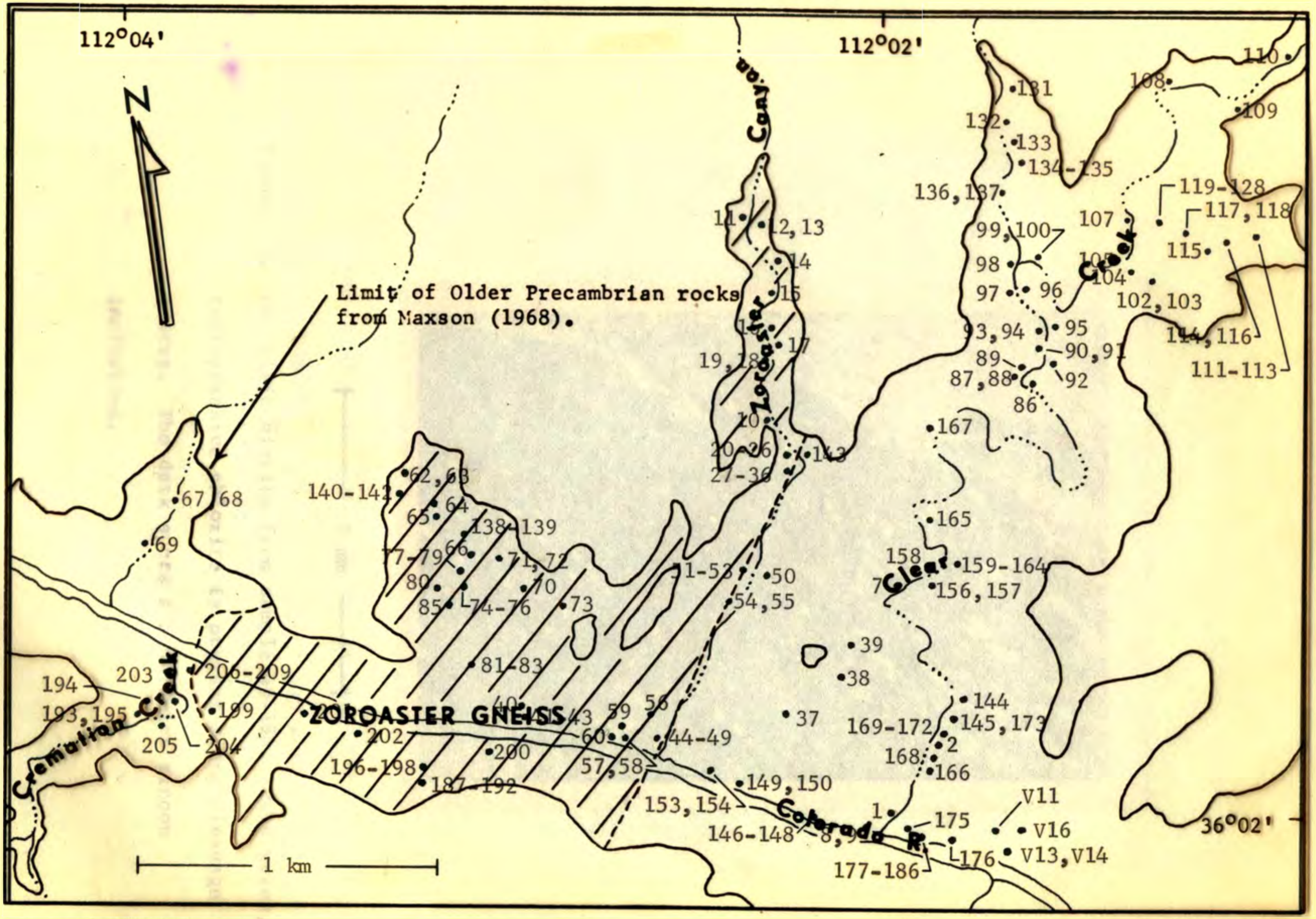

Figure 2. Map of the Clear Creek-Zoroaster Canyon area showing sample locations.

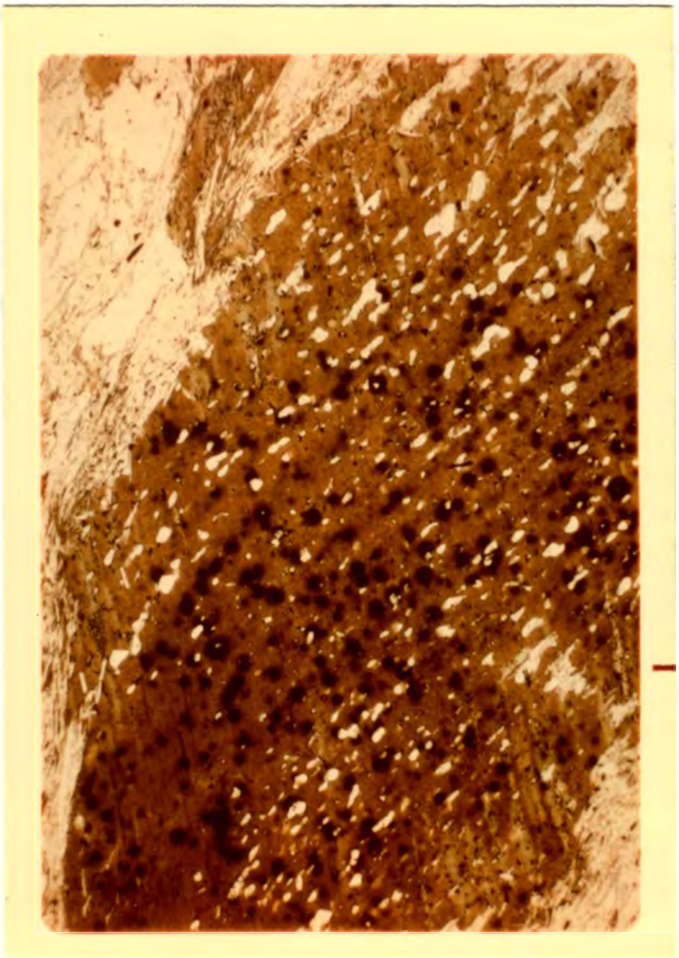

3 mm

Figure 3. Helicitic biotite from sample 46-184. Pale green, retrogressive chlorite is present along cleavage traces. The dark spots are metamict zircon inclusions.

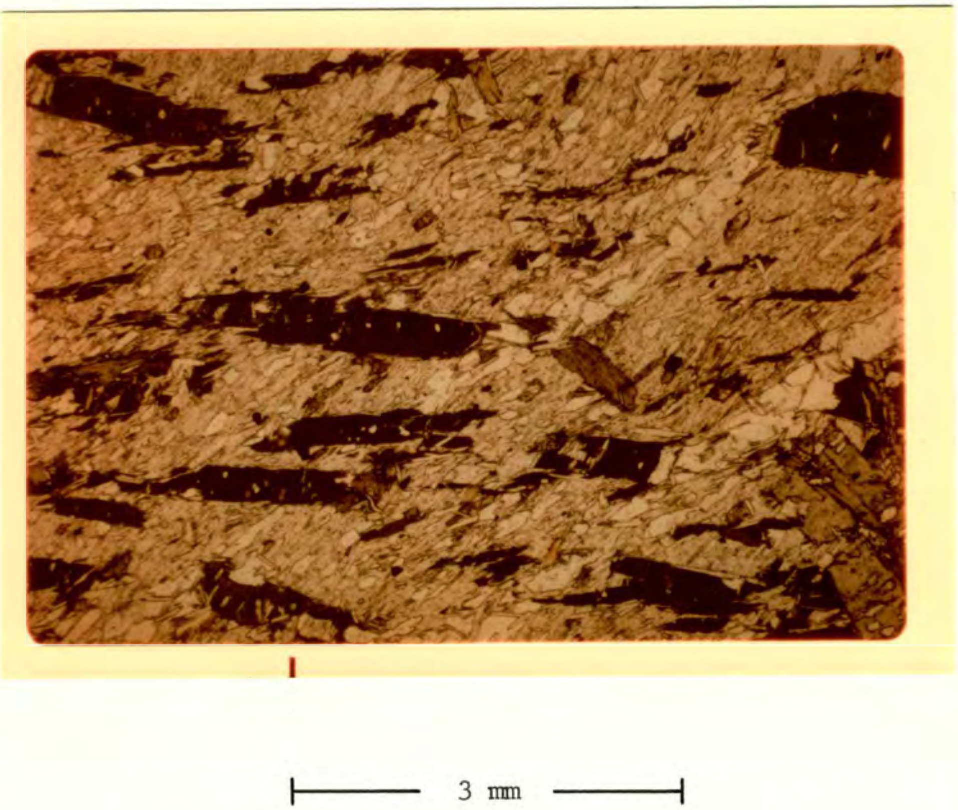

Figure 4. Photomicrograph of sample 46-182 showing two foliations. S_1 is defined by fine grained muscovite and biotite and S_2 by the large biotite porphyroblasts.

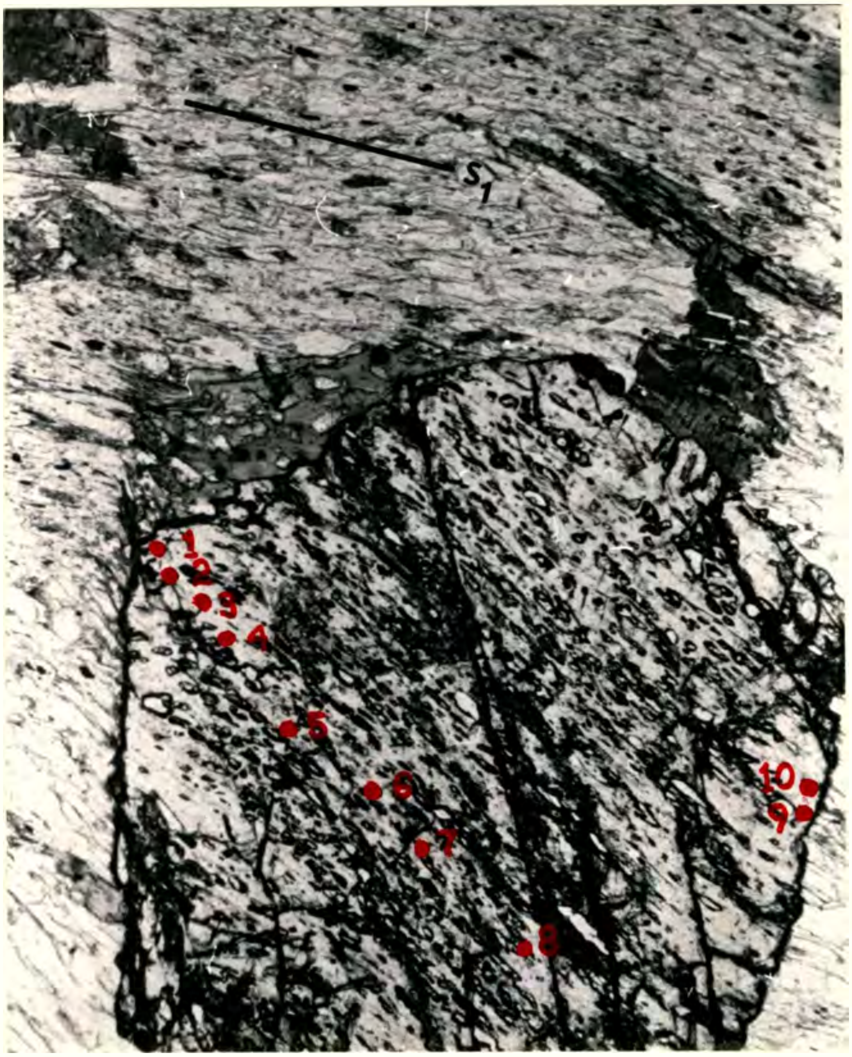

3 mm

Figure 5. Garnet from sample 46-184. The numbered points above refer to corresponding microprobe traverse data given in Table 1. Note straight inclusion trails at an angle to the general trend of S_1.

Table 1. Microprobe analysis data for individual minerals from samples 46-183 and 46-184. Analyses by E. H. Brown.

Sample	Wt. % MgO	Wt. % FeO*	Wt. % CaO	Wt. % Al_2O_3
183 Biotite 1	8.15	21.65	0.00	20.49
183 Biotite 2	8.24	22.04	0.00	20.20
183 Muscovite	0.56	1.11	0.00	35.90
183 Chlorite 1	11.14	29.16	0.00	22.48
183 Staurolite	1.40	13.56	0.03	57.03
183 Opaque	0.19	37.34	0.06	0.00
184 Chlorite in Biotite	11.30	30.39	0.00	18.41
184 Biotite 1	8.57	21.26	0.00	18.48
184 Biotite 2	9.07	21.68	0.00	18.66
184 Chlorite	10.35	26.56	0.00	19.43
184 Muscovite	0.61	1.01	0.00	37.01
184 Garnet Point 1	1.75	37.50	2.13	19.26
184 Garnet Point 2	1.87	37.01	2.29	19.66
184 Garnet Point 3	1.95	36.96	2.17	19.50
184 Garnet Point 4	1.87	36.23	2.54	19.69
184 Garnet Point 5	1.66	35.17	2.60	19.68
184 Garnet Point 6	1.48	34.15	2.69	19.61
184 Garnet Point 7	1.42	34.11	2.69	19.51
184 Garnet Point 8	1.16	35.80	2.80	19.40
184 Garnet Point 9	1.50	37.24	1.53	20.79
184 Garnet Point 10	1.25	37.35	1.58	20.63

* All Fe as FeO.

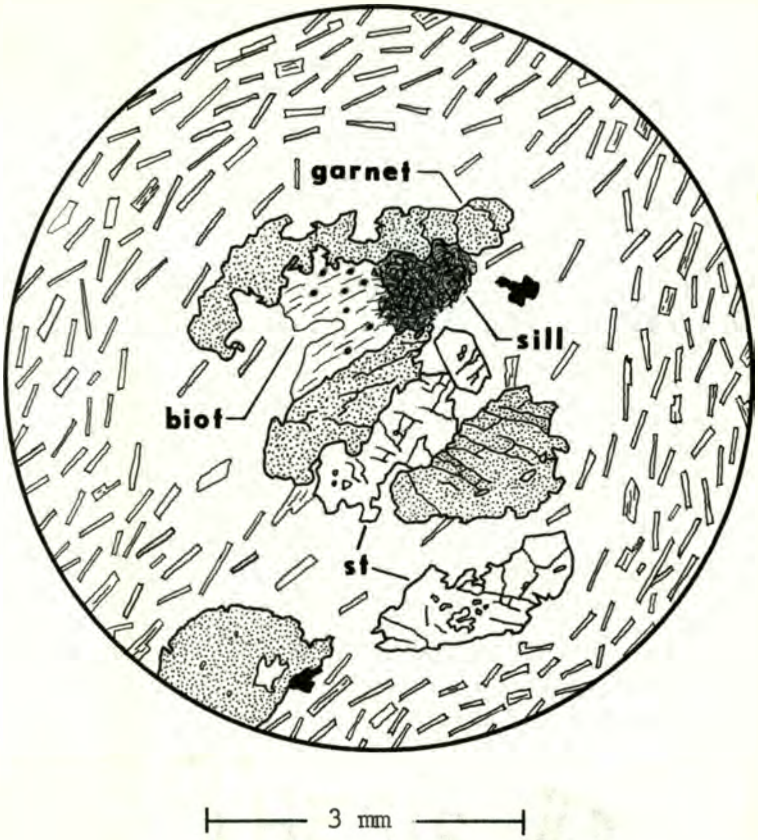

Figure 6. Relationship of garnet, staurolite, biotite and sillimanite in sample 46-169.

3 mm

Figure 7. Porphyroblastic staurolite from sample 46-176.

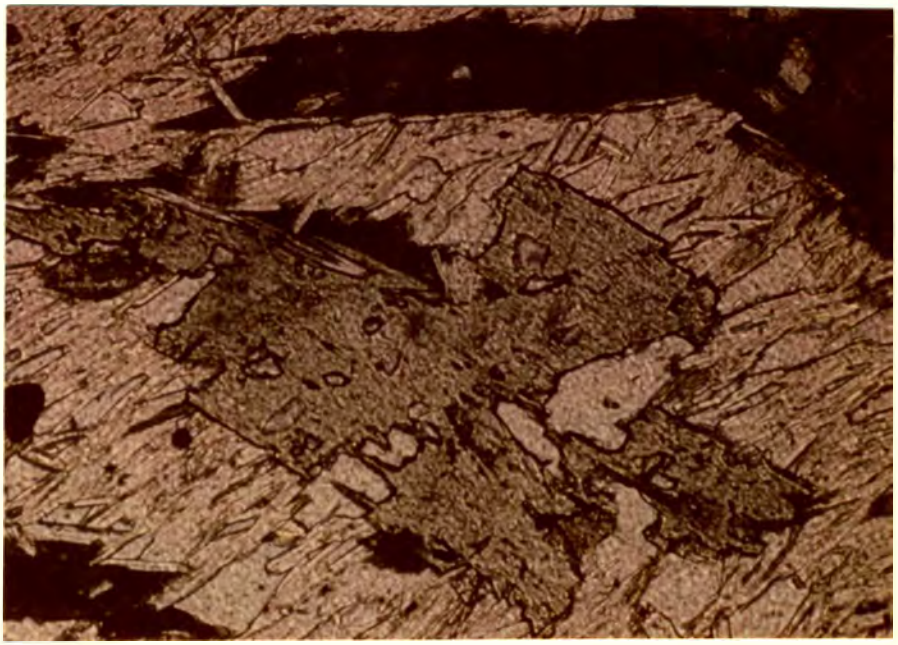

3 mm

Figure 8. Over-printed chlorite from sample 46-V14. The dark minerals which over-print the foliation are biotite porphyroblasts.

Sillimanite

The fibrous sillimanite present in these rocks is everywhere associated with biotite, and some textural evidence suggests that biotite is being replaced by sillimanite. The amount of sillimanite in thin section varies from a few individual fibers to felts which may occupy one percent of the volume. A few individual fibers of sillimanite radiate from the ends of some biotites. Other biotites appear to be replaced by sillimanite to such an extent that only a pleochroic patch remains. C-crystallographic axes of the sillimanite are parallel to the cleavage traces of the biotite. Zircon inclusions may be traced from biotites, through intermixed biotite and sillimanite, and into sillimanite felts with no biotite whatsoever. The large felts of sillimanite definitely over-print the schistosity. Many similar occurrences of sillimanite have been reported (Chakraborty and Sen, 1967; Chinner, 1961; Francis, 1956; and Tozer, 1956).

Other Minerals

Muscovite constitutes 15 to 75 percent of the mode of the micaceous schists and occurs as pretectonic or syntectonic plates. Quartz is equidimensional and granular. It generally shows undulose extinction and a small 2V. Plagioclase also shows undulose extinction and deformation twins are common. Plagioclase compositions range from An_{24} to An_{35} as determined by the a-normal method. A few samples were checked with the universal stage method (Slemmons, 1962) and their compositions were An_{28}. Post tectonic, albitic porphyroblasts were observed in sample 46-176. These cross-cut the foliation at a 30° angle.

Pleochroic green tourmaline comprises as much as one percent of the volume of some samples. Tourmaline in a schist outcrop, in Zoroaster Canyon appears to have been metasomatically introduced by fluids from an adjacent tourmaline-rich pegmatite dike. Numerous euhedral and anhedral opaques are present in these rocks. They range up to 2.5 mm in diameter. Microprobe analysis has shown that ilmenite and hematite are present. Zircon appears as very small grains, and more commonly as metamict inclusions in biotite and muscovite (see Figure 3).

Amphibolite

Amphibolite crops out at Clear Creek, Cremation Creek, and sporadically through the Zoroaster Gneiss. At Clear Creek, vertical layers of amphibolite range in thickness from a few centimeters to more than 100 meters. The largest layers are located 2500 and 4000 m upstream from the Colorado River. They strike parallel to the lithologic layering and foliation of the surrounding schists. Amphibolites are poorly foliated here. Amphibolite also crops out as smaller metamorphosed mafic sills with a well developed foliation concordant with the schist foliation. There is some possibility that these two types represent separate generations of mafic volcanism or intrusion.

Within the Zoroaster Gneiss, amphibolite crops out as large, metamorphosed mafic sills and unusual flake-like structures. The flake-like structures are located just east of Cremation Creek and about 200 m above the Colorado River (Figure 9). They appear to be part of an intertonguing contact between the gneiss and a large, obscured amphibolite body. These structures display a radiating pattern which spreads out towards the east. The flake-like structures and the surrounding gneiss are folded on a mesoscopic scale in several locations are part of a macroscopic anticlinal or dome structure (see macroscopic folding and Figure 9). The thickness of individual 'flakes' range from 0.5 to 10 m and their lengths are as much as 250 meters.

Two possibilities exist for the origin of the flake-like structures. They may represent ragged septa of a foliated amphibolite body which has been intruded by Zoroaster magma. After the magma was emplaced around these septa, it developed a schistosity parallel to the amphibolite foliation. Later, both the amphibolite septa (flakes) and the gneiss were macroscopically folded. This hypothesis requires two generations, or at least separate pulses of mafic magma because large amphibolite sills are found intruding the Zoroaster Gneiss in several locations.

The second possibility is that the amphibolite intruded the Zoroaster Gneiss as a mafic magma. This hypothesis is supported by a compositional similarity to the mafic sills which intrude the gneiss. This similarity suggests that there was only one generation of mafic magma. Unfortunately, many crucial outcrops were obscured or inaccessible and more field work will be required to ascertain the relationship of the gneiss and amphibolite.

At Cremation Creek, amphibolite constitutes approximately 50 percent of the outcrop volume. The remainder is intermixed pegmatite and aplite (Figure 10).

Two of the metamorphosed mafic sills within the Zoroaster Gneiss are remarkable. Their thicknesses are 0.5 and 8 m respectively, and they are a minimum of 2000 m in length. North of the Colorado River they are vertical, strike northeast, and display marked pinch and swell structure. South of the Colorado River they are folded into a huge east-west arc along with the flake-like structures and the Zoroaster Gneiss (see Figure 9). The foliation in these and other, smaller, metamorphosed sills is everywhere concordant with the adjacent gneissosity.

Amphibolite in the Clear Creek drainage is thoroughly intermixed with the metasediments. For this reason, the present writer agrees with Ragan and Sheridan's suggestion that the name Brahma Schist for the amphibolites is unwarranted.

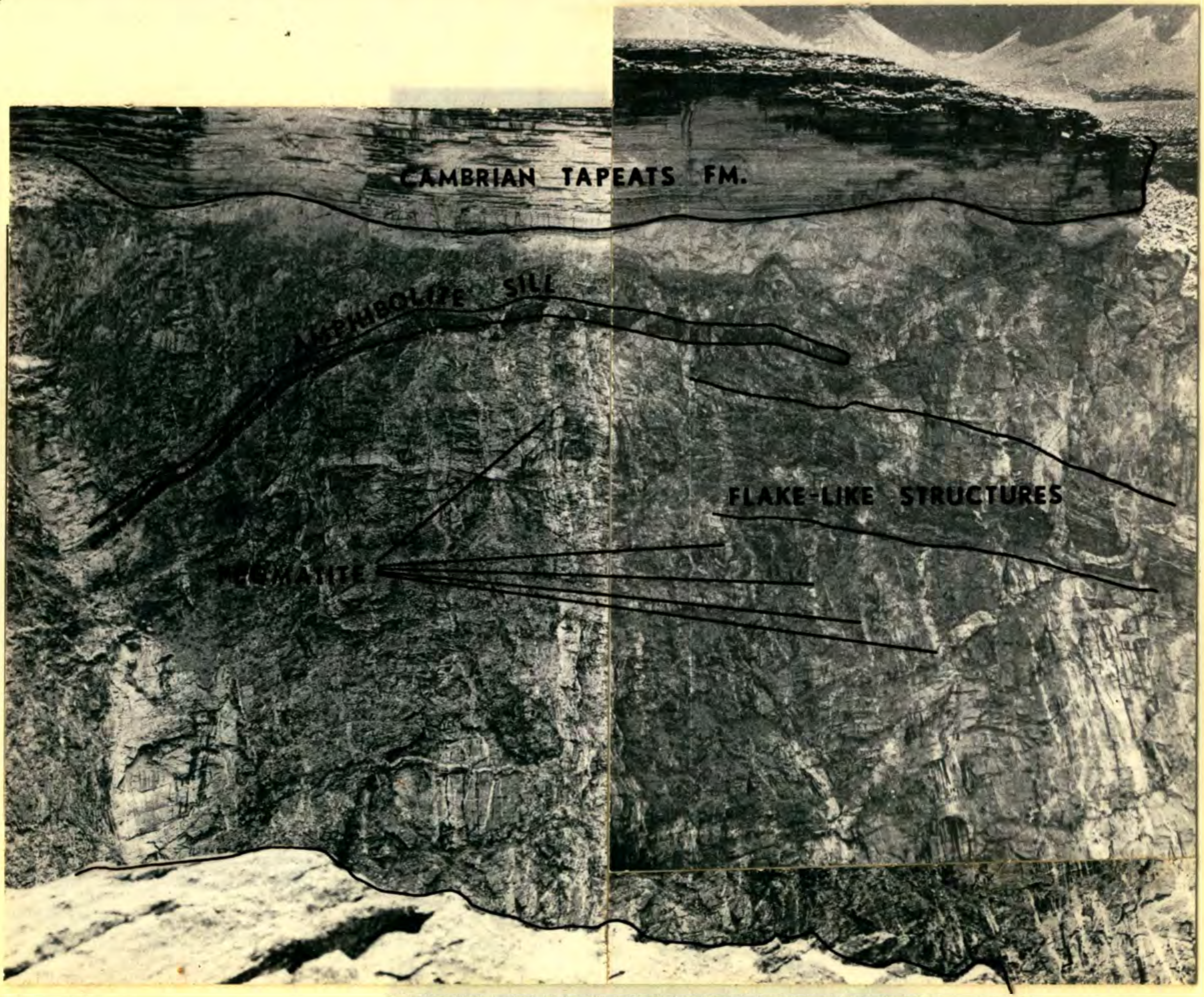

Figure 9. View showing the south side of the Inner Gorge of the Colorado R. from mile 85.1 to 85.8.

0.5 km

Figure 10. Light colored pegmatite and aplite intrusions in darker amphibolite at the east side of Cremation Creek canyon. These rocks are overlain by the Cambrian Tapeats Fm.

The following mineral assemblages were observed in amphibolites:

hornblende-oligoclase-sphene-apatite-opaque±biotite± quartz±epidote±actinolite

These assemblages are similar to those found in amphibolites derived from mafic igneous rocks (Williams, Turner, and Gilbert, 1954). The mineralogical homogeneity seen in all of the amphibolite samples is further evidence for an igneous parent.

Schistosity is usually weakly developed in these samples. Epidote-chlorite layers are common Clear Creek and these are intercalated with amphibolite on a scale of one or two cm. No textural evidence of prograde reactions is present.

The amphibole in most of these assemblages as determined by optical properties and the tables of Heinrich (1965) is ferrohastingsitic hornblende. Patchy zoning characterized by color variation has been observed in assemblages containing biotite. Idioblastic hornblende constitutes 35 to 55 percent of the mode of the amphibolites. Individual crystals are as large as 3 mm.

Plagioclase compositions determined by the a-normal method range from An_{26} to An_{34}. Plagioclase and quartz show undulose extinction and granulated grain boundaries. Deformation twins in plagioclase and a small 2V in quartz are further evidence of late deformation. Where present, biotite makes up less than one percent of the sample. Biotite-rich assemblages have only been noted in samples of the altered amphibolite-pegmatite/aplite contact at Cremation Creek. Chlorite, and chlorite+potash feldspar commonly pseudomorph biotite.

Meta-calcsilicates

Meta-calcsilicate layers and lenses are common in the Clear Creek drainage. Two varieties can be discerned in hand specimen; deep green layers rich in epidote and lighter green to white layers in which calcite is the predominant mineral. The latter variety is particularly well exposed at the mouth of Clear Creek where layers 6 to 35 cm thick form F_1 folds (see Mesoscopic Folding). The dark green variety lacks distinct boundaries and is commonly associated with amphibolite masses. These layers range from a few centimeters to several meters in thickness.

Assemblages which were observed in thin sections of calcite-rich rocks include the following:

1) calcite-plagioclase-quartz-hornblende-garnet-sphene-opaques-chlorite

2) calcite-hornblende-sphene-opaques

The only assemblage noted in the dark green variety was garnet-opaque-hornblende-epidote-quartz-calcite-plagioclase-apatite-zircon.

Garnets have an orange tint indicative of a grossularite-rich composition and are generally fine grained. Within individual layers, coarse grained epidote, euhedral opaques, and grossularite-rich garnet are segregated into thin bands, some of which show boudinage structure.

Metamorphism and Metamorphic Grade

The textural and mineralogical relationships described in the preceding sections indicate several phases of metamorphism. These phases of metamorphism are defined by the appearance of new metamorphic minerals through prograde and retrograde reactions. The following discussion will deal with the micaceous schists because similar schists elsewhere have been carefully studied and their reactions are well understood.

Three groups of minerals have been recognized in these rocks: remnants of a pretectonic and syntectonic assemblage, a post tectonic prograde assemblage, and a post tectonic retrograde assemblage. Several schist samples contain the following nine mineral phases: quartz, plagioclase, muscovite, biotite, chlorite, garnet, staurolite, fibrous sillimanite, and fluid. The eight major chemical components in this system are SiO_2, Na_2O, K_2O, MgO, H_2O, FeO, CaO, and Al_2O_2. This violation of the mineralogical phase rule (components = phases at divariant equilibrium) may be explained by an invariant assemblage. Another possible explanation is that some of the mineral phases have resulted from incomplete prograde and/or retrograde reactions. The following discussion will suggest specific possibilities for the genesis of these minerals and define the metamorphic grade.

Remnants of the synkinematic and/or pretectonic assemblage include the biotite and muscovite which parallel the schistosity and a few synkinematic, sigmoidal garnets. All of the garnets in these rocks are thought to have formed by the time the schistosity was completely developed. Many of the garnets are pretectonic relicts as indicated by straight inclusion trails at an angle to the schistosity. None over-print the schistosity.

The prograde minerals recognized in these rocks are biotite, staurolite, and fibrous sillimanite. Reactions where biotite or biotite + garnet are the products are so numerous that no attempt will be made here to suggest a specific reaction. The biotite, which forms the secondary foliation seen Sample 46-182, may have simply dissolved and reprecipitated in response to realigned directed stress.

Biotite developed along fractures in garnets may be the result of retrograde reactions.

Staurolite generally appears as a pretectonic or syntectonic mineral. Poikiloblastic staurolite commonly occurs with corroded garnets, quartz, and biotite at sites originally occupied by larger garnet porphyroblasts (see Figure 6). A staurolite producing reaction, derived by Thompson and Norton (1968), that fits this textural relationship is:

almandine + chlorite + muscovite $\longrightarrow$ staurolite + biotite + quartz + H_2O

In several other samples, staurolite appears to have formed independently of garnet. A reaction consuming chloritoid may have been responsible for the first appearance of staurolite in these rocks. Possible chloritoid-staurolite reactions are:

54 Chloritoid + 5 O_2 $\longrightarrow$ 12 Staurolite + 10 Magnetite + 6 Quartz + 48 H_2O (Ganguly, 1968)

Chloritoid + Quartz $\longrightarrow$ Staurolite + Al + H_2O (Ganguly, 1969)

Ganguly (1972) has found that the lower limit of staurolite stability is $500^{\circ}C$ to $575^{\circ}C$ in reactions where chloritoid is a reactant.

After staurolite was formed, the phase relationships of these rocks would be as shown in Figure 11a, an AFM projection, after Carmichael (1970) and others. These phase relationships are based on the assumption that all chlorite was consumed in lower grade reactions and that staurolite, as all the textural evidence suggests, is a stable phase.

Fibrous sillimanite was one of the last post-tectonic, prograde minerals to form. Numerous similar occurrences of sillimanite and biotite have been reported (see page 19). Recent work by Chinner (1961) and Chakraborty and Sen (1967) indicates that biotite is a structurally favorable site for sillimanite nucleation. Biotite should not be involved in a sillimanite reaction because it is not an aluminum excess mineral (aluminum excess being defined as more Al than is necessary to form feldspars: $Al/Na+K+2Ca > 1$). Chinner has noted the relationships of zircon with sillimanite and biotite mentioned in the micaceous schist section of this paper. But, he concludes that any reaction involving the destruction of biotite to form sillimanite is an intermediate step.

These rocks are thought to have reached a maximum of sillimanite zone metamorphism. Here, the three phase assemblage sillimanite-biotite-staurolite is stable. At slightly lower grade, kyanite is the stable Al-silicate and at higher grade the stable assemblage is sillimanite-garnet-biotite (Carmichael, 1970). Staurolite is thought to be stable in these rocks because of its sharp grain boundaries and fresh appearance. Garnet, on the other hand, has a corroded outline and only small patches remain where large porphyroblasts were present.

Sillimanite may have formed directly from kyanite at this grade. However, a possible explanation for the textural implication that biotite is a reactant in the sillimanite-forming reaction would be a simple redistribution of Mg and Fe in these phases. For example, assume a hypothetical bulk composition for these rocks at point X in Figure 11a. If the assemblage biotite-garnet-staurolite were to undergo a redistribution of Mg and Fe, such that all three phases were enriched in Fe, then the sillimanite-staurolite-biotite three phase field would shift over the bulk composition point (Figure 11b) and sillimanite would be formed.

Another hypothesis is that sillimanite formed in the sillimanite-biotite-garnet zone and that the corroded garnets indicate a retrograde reaction to form staurolite. A reaction which seems to fit the textural data is:

$$\text{almandine} + 12 \text{ sillimanite} + \text{biotite} + H_2O \longrightarrow \text{staurolite} + \text{muscovite} + 4 \text{ quartz} \quad \text{(Carmichael, 1970)}$$

Although there has been considerable discussion in the literature about the formation of fibrous sillimanite, the problem is poorly understood. The possibility exists that the fibrous variety of sillimanite can form at a somewhat lower grade.

Chlorite is obviously a post-tectonic, retrogressive phase and it is nearly ubiquitous. Pseudomorphs of chlorite and chlorite+potash feldspar after biotite and/or garnet suggest obvious reactions. The large number of fresh, over-printing, patches of chlorite show that the retrogressive phase was a major metamorphic event.

Distribution coefficient values for MgO/MgO+FeO in garnet-biotite pairs from sample 46-184 show that the retrogressive phase was characterized by biotite or garnet zone metamorphism. Partitioning of MgO and FeO in these minerals is a continuous function of metamorphic grade; the K_d value increases continuously with increasing metamorphic grade (Albee, 1965; Brown, 1969; Lyons, 1970; and Heitanen, 1969). K_d values from the rim of the garnet in 46-184 and an adjacent biotite range from 0.08 to 0.12. Correlating specific grade with its associated K_d value is difficult because K_d values are affected by other aspects of garnet composition (Albee, 1965). K_d values which correspond with garnet zone metamorphism, as determined by others, are 0.20-Albee, 0.09-0.12-Brown, 0.10-Lyons, and 0.11-Heitanen. All garnet-biotite K_d values which were calculated are given in Table 2.

Distribution coefficient data was also used as a test of equilibrium for the over-printed chlorite. K_d values were obtained from chlorite pseudomorphs after biotite and remnants of the biotite. The values for these pairs, clearly at disequilibrium, were 0.88 and 0.92. Distribution coefficient values for chlorite-biotite pairs at equilibrium do not vary appreciably from 1.0 according to Brown (1969) and Albee (1968). Values for the over-printed chlorites and associated fresh-appearing biotites in sample 46-183 and 46-184 are 1.01, 1.02, and 0.96. Presumably these values indicate that the retrogressive metamorphism was strong enough to carry some chlorite producing reactions to equilibrium.

In summary, the Vishnu Schist developed its present mineral assemblage in three phases. The pretectonic and/or syntectonic minerals are biotite, muscovite, chlorite, and garnet (+chloritoid?). The prograde minerals are biotite, staurolite and fibrous sillimanite and the post-tectonic retrograde minerals are chlorite and biotite. The highest grade attained in the post-tectonic prograde phase is thought to have been in the sillimanite-biotite-staurolite zone. The temperatures involved were probably in excess of 600°C.

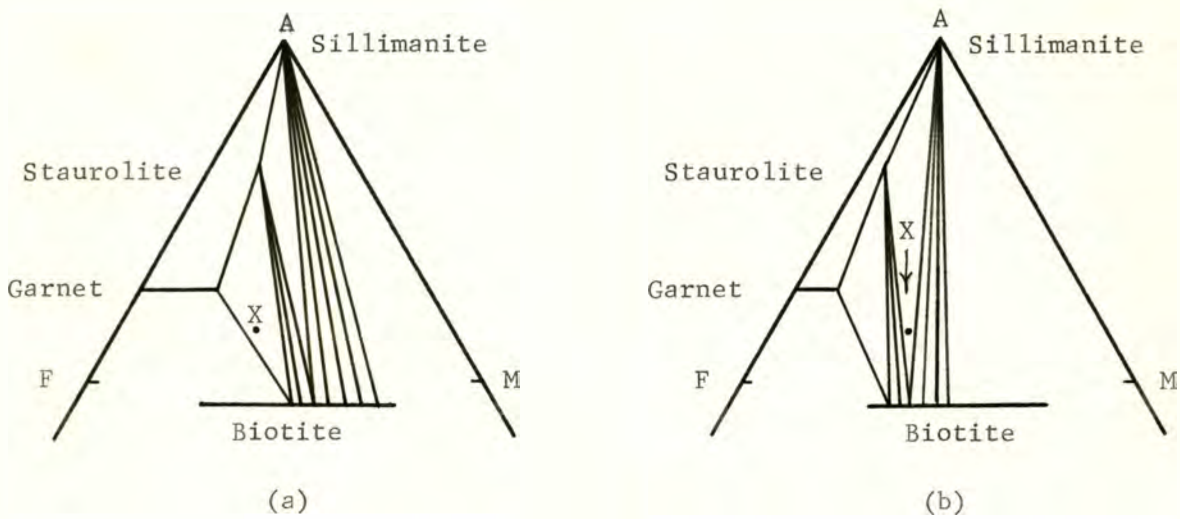

Figure 11. Interpretation of phase relations of sillimanite zone pelitic schists from Clear Creek. (a) Some sillimanite zone phase relations observed by Thompson and Norton (1968), Carmichael (1970), and Albee (1972). The assemblage staurolite-biotite-garnet would be stable in a rock with a bulk composition X at this grade. (b) These same phases enriched in their Fe-component. In a rock with composition X, garnet breaks down to form a sillimanite-biotite-staurolite assemblage during the shift to more Fe-rich mineral compositions.

Table 2. Distribution coefficients for Mg/Mg+Fe in coexisting biotite and garnet from sample 46-184.

Sample	K_d
Biotite 1 / Garnet Point 1	0.116
Biotite 1 / Garnet Point 2	0.126
Biotite 1 / Garnet Point 3	0.130
Biotite 1 / Garnet Point 4	0.128
Biotite 1 / Garnet Point 5	0.117
Biotite 1 / Garnet Point 6	0.106
Biotite 1 / Garnet Point 7	0.103
Biotite 1 / Garnet Point 8	0.117
Biotite 1 / Garnet Point 9	0.100
Biotite 1 / Garnet Point 10	0.083
Biotite 2 / Garnet Point 1	0.112
Biotite 2 / Garnet Point 2	0.122
Biotite 2 / Garnet Point 3	0.126
Biotite 2 / Garnet Point 4	0.123
Biotite 2 / Garnet Point 5	0.113
Biotite 2 / Garnet Point 6	0.104
Biotite 2 / Garnet Point 7	0.099
Biotite 2 / Garnet Point 8	0.112
Biotite 2 / Garnet Point 9	0.096
Biotite 2 / Garnet Point 10	0.080

THE ZOROASTER GNEISS

The Zoroaster Granite is defined by Maxson (1968) as pink, microcline-rich granite. His type locality is the large monadnock west of Zoroaster Canyon, the west side of the present study area. At this location, the name Zoroaster Gneiss would be more accurate and should be used in the future since most of the rock displays a strong, pervasive foliation. This name will be used in the present report.

The Zoroaster Gneiss is composed of two major phases: a pink, biotite gneiss and a fine grained, poorly foliated gneiss. The composition of both phases is muscovite-biotite granodiorite. The fine grained phase and non-foliated granitic rocks in the monadnock make up less than 15 percent of the outcrop volume. Maxson (1968) included the pegmatite, aplite, and non-foliated granodiorite which cut the gneiss in this unit. The present writer believes that these rocks are much later phases and should not be included with the Zoroaster Gneiss.

Zoroaster Gneiss is exposed on both sides of the Colorado River west of Zoroaster Canyon and covers about 1 km^2. North of the Colorado River, the gneiss crops out as the aforementioned monadnock overlain by Paleozoic strata. Here the foliation is vertical and strikes northeast, whereas south of the Colorado River the foliation is folded into a huge anticlinal structure. Foliation is as well developed at the center of the gneiss as it is at the margins. There is no evidence that the foliation is a igneous flow structure.

Shear zones parallel to the foliation are common and shear zones which cut the foliation at large angles have been observed.

Several shear zones display a bifurcating pattern. Mafic schlieren are concentrated in many of these shear zones and partially assimilated xenoliths are present throughout the gneiss. The foliation and shear zones commonly continue into pegmatite and/or aplite which cut the gneiss (Figure 12).

The contact between the fine grained gneiss and the coarse grained, main-stage, gneiss is gradational and indistinct. Both phases are intruded by numerous pegmatite and aplite dikes and sills.

24 cm

Figure 12. Zoroaster Gneiss cut by a typical pegmatite dike from upper Zoroaster Canyon. Note the pure quartz masses at the center of the dike and gneissosity which continues into the margins of the dike.

The major mineral phases in the Zoroaster Gneiss are microcline, plagioclase, quartz, muscovite, and biotite. Zircon, apatite, tourmaline, hematite and other opaques are common accessory minerals. Microcline appears as grid twinned prisms and microperthitic intergrowths with albite or oligoclase. Granophyric textures are very common and myrmekitic intergrowths of quartz and plagioclase have been observed.

Modal analyses of granitic rocks were made using the technique of Chayes (1962) with a minimum of 1300 counts per sample. The results of these analyses are given in Table 3 and shown graphically in Figure 13. The amount of microcline in the gneiss varies from 3 to 31 percent of the mode.

Plagioclase compositions range from An_7 to An_{28} though most samples are albitic. Three methods of determination were used: a-normal, universal-stage method of Slemmons (1962), and by conversion of microprobe analysis data.

Muscovite makes up as much as 12 percent of some samples and biotite constitutes 7 percent of the mode of others.

A strong foliation is developed in all samples of main stage gneiss and no minerals over-print the foliation. Late deformation textures are developed in every sample. Mortar texture is prevalent and plagioclase and quartz show strain textures. All the textures observed in these rocks are metamorphic; no relict igneous textures were noted.

All gneiss samples have a strong pink color due to abundant microscopic hematite disseminated throughout the feldspar grains and along mica cleavage traces.

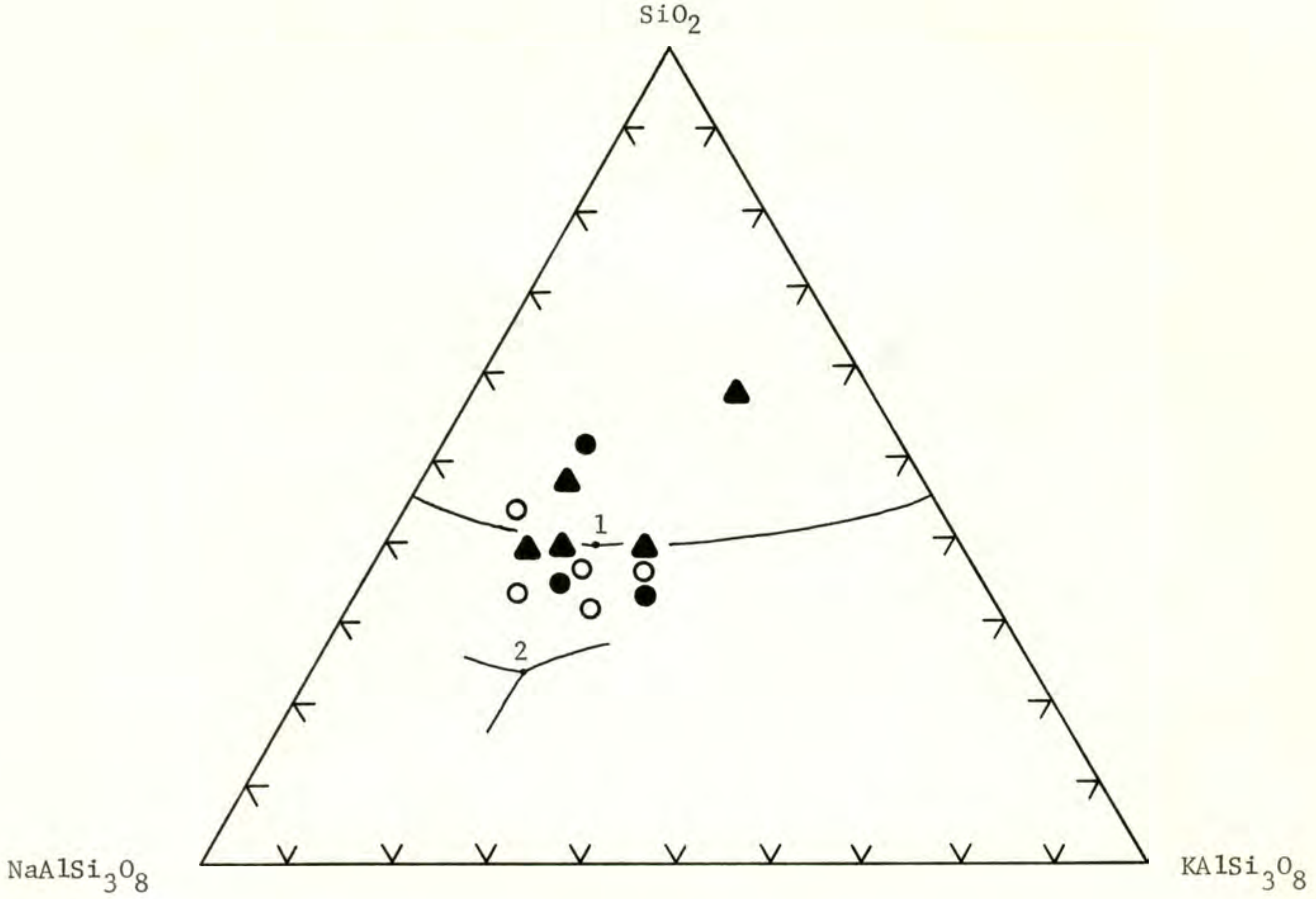

Figure 13. Modal analyses of Zoroaster Gneiss (triangles), aplite (open circles), and late granitic rocks (closed circles). Point 1 is the isobaric minimum melt for the system Ab_{90}-Or-Q-H_2O at P_{H_2O} = 2000 bars (modified after Von Platen, 1965). It should be noted that this is not a eutectic as suggested by Von Platen (Weill and Kudo, 1968). Point 2 is the eutectic for the system Ab_{100}-Or-Q-H_2O at P_{H_2O} = 5000 bars (after Luth et al., 1964).

The Vishnu Schist-Zoroaster Gneiss Contact

The Vishnu Schist-Zoroaster Gneiss contact is located along the west slope of lower Zoroaster Canyon (see Figure 2). The contact dips 68 to 85° east. Lithologic layering in the schist, and the contact are parallel and nearly straight for 1500 m along Zoroaster Canyon. Foliation in the schist and the gneiss is everywhere parallel. The contact is particularly sharp and well defined. There is no evidence of faulting. Lithologic layering, schistosity and gneissosity, and the contact are all warped by late deformation.

Large, tabular blocks of schist are common, immediately west of the contact inside the gneiss (Figure 14). These blocks strike parallel to the contact and dip between 55 and 75° east. They vary from 6 to 10 m in thickness and extend tens of meters in length before they are obscured by the surrounding gneiss. Foliation in the blocks is generally sub-parallel to gneiss foliation. Small apophyses intrude the schist blocks and schist east of the contact at several locations. Undisturbed foliation can be traced from the gneiss apophyses, across the contact, and into the schist.

The dominant lithologies on the east side of the contact, within the schist, are monomineralic muscovite and biotite rocks, altered mica schist, and chlorite-biotite-garnet schist. The latter is in direct contact with the gneiss where Zoroaster Canyon turns west, 1300 m north of the Colorado River. Although the gneiss is grayer in color and displays an altered aspect at the contact, there is nothing in thin section to distinguish it from samples collected further west. The tabular schist blocks described above are felsic in comparison with the schist east of the contact and they show a rough gradational relationship with the gneiss. Quartz veins up to two meters in thickness and a few pegmatite dikes cut the contact.

Table 3. Modal analyses data.

Sample	Rock Type	% Plagioclase	% Quartz	% K-Feldspar
46-11	gneiss	33.6	38.2	28.2
46-12	aplite	33.8	36.5	29.7
46-20	aplite	40.6	36.3	26.1
46-65	gneiss	13.6	57.7	28.7
46-75	gneiss	43.4	44.2	12.4
46-80a	late granitic	32.7	51.3	16.0
46-80b	late granitic	43.2	34.9	21.9
46-82	late granitic	35.2	33.6	31.3
46-85	aplite	36.8	47.3	15.9
46-138	gneiss	41.8	39.6	18.6
46-157	gneiss	44.4	38.4	16.0
46-190	aplite	41.6	32.6	25.8
46-209	aplite	48.2	33.1	18.7

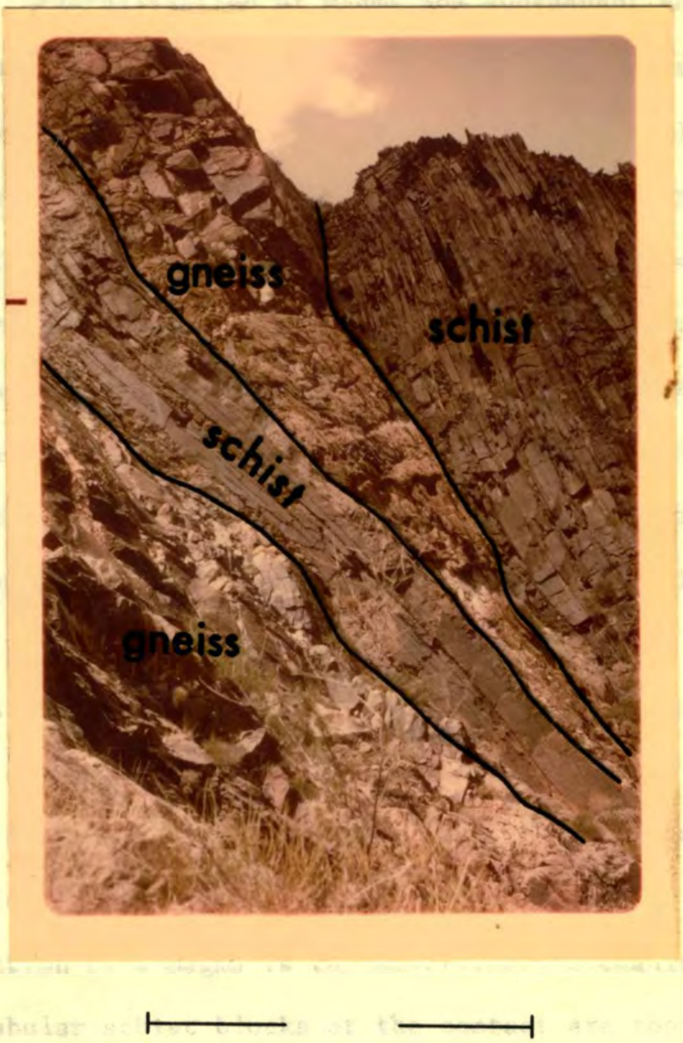

Figure 14. View looking north to the Vishnu Schist-Zoroaster Gneiss contact in lower Zoroaster Canyon.

Origin and Emplacement of the Zoroaster Gneiss

Hypotheses for the origin and emplacement of the Zoroaster Gneiss include the following: 1) crystallization from a magma followed by late deformation, 2) crystallization of magma and subsequent emplacement as a gneiss dome, 3) in situ anatextis of the Vishnu Schist, 4) metasomatic replacement of the Vishnu Schist (granitization).

The last two hypotheses are unlikely because of the sharpness of the Vishnu Schist-Zoroaster Gneiss contact and because the contact is very straight for 1500 m along Zoroaster Canyon. A granitic gneiss, which formed in situ by a metasomatic or anatectic process, would undoubtedly show gradational contacts with the host rock. Fragile structures at the contact such as the tabular schist blocks and gneiss apophyses are evidence against emplacement as a gneiss dome. It is unlikely that rocks in a viscous plastic state, as required by the gneiss dome hypothesis, could form these intricate injection features. The lack of reverse drag folds at the margins of the Zoroaster Gneiss is further evidence against the gneiss dome hypothesis (D.A. Rahm, personal communication).

Forceful injection of a magma is the most likely mechanism of emplacement. The tabular schist blocks at the contact are thought to be a complex injection zone. The straightness of the contact can best best be explained by intrusion along a pre-existing plane of schistosity or lithologic layering.

Modal analysis data supports a magmatic origin for the gneiss. The cotectic lines and minimum melt point for the system Ab_{90}-orthoclase-quartz-H_2O are plotted on Figure 13 (after Winkler, 1967). Most of the gneiss samples fall very close to the minimum-melt thermal trough. This fact is strong evidence that these rocks formed under conditions of crystal-melt equilibrium. It also suggests one of the following origins for the magma: 1) the magma formed by anatexis and was subsequently injected into its present location, or 2) the magma represents the last liquid portion of a much larger magma mass.

The time relationship between the deformation which created the foliation in the Vishnu Schist and the hypothesized magma injection is a matter of conjecture. The writer believes that the magma was synkinematically injected along a pre-existing foliation plane. If that is the case, deformation must have out-lasted plutonism by enough time to creat the gneissosity. There is a possibility that the magma was injected along a plane of lithologic layering prior to deformation. In this case, foliation in the schist and gneiss would have formed synchronously.

PEGMATITE AND APLITE

Pegmatite and aplite sills and dikes are exposed throughout the study area, though only a few are present in the eastern half. The total volume of pegmatite and aplite increases towards the western margin of the study area. Here, pegmatite and aplite constitute 30 to 45 percent of the outcrop volume.

Aplite shows a broad variety of relationships with pegmatite (Figure 15). Aplite and pegmatite are commonly found in dikes which are symmetrically zoned. These dikes may show as many as six separate layers of aplite and pegmatite. Some dikes have pure quartz segregations in their centers. Dikes and sills of pure aplite or pegmatite are also abundant. At Cremation Creek, aplite is randomly intermixed with pegmatite in dikes up to 65 m in width.

Dikes of pegmatite and/or aplite show complex crosscutting relationships with each other. Aplite dikes cut both pegmatite dikes and other aplite dikes. As many as four pegmatite dikes are superimposed, one cutting another. Pegmatite dikes and zoned pegmatite/aplite dikes crosscut aplite dikes. Quartz veins cut and are cut by aplite/pegmatite dikes. A leucotrondjemitic dike cuts pegmatite dikes 250 meters up Cremation Creek.

These crosscutting relationships could result from several generations of pegmatite/aplite, but strong similarities in composition and occurrence suggest that most pegmatite and aplite dikes are genetically related. A few weakly foliated pegmatite dikes may be related to the Zoroaster Gneiss.

Contacts between amphibolite and pegmatite/aplite dikes are everywhere sharp and well defined; however, narrow alteration zones occur at the contacts. In these zones, amphibolite has altered to chlorite-garnet schist. A particularly well developed alteration zone is found 600 m up Cremation Creek at the largest waterfall. Feldspar has penetrated the amphibolite up to 7 cm from the contact. The pegmatite at the contact has a distinct mafic aspect and metasomatic replacement is implied. Biotite, which was originally present in the replacement zone amphibolite has been pseudomorphed by chlorite+potash feldspar.

Pegmatite/aplite generally truncates amphibolite foliation but pegmatite/aplite sills are present also. Numerous pegmatite/aplite dikes a few centimeters wide and many meters in length intrude the amphibolite. A rotated xenolith of amphibolite suspended in pegmatite was observed at Cremation Creek (Figure 16). The foliation in any two amphibolite masses separated by pegmatite is subparallel, but the geometrical relations displayed by these amphibolite masses suggest that dilational movement has taken place as a result of pegmatite/aplite intrusion.

The sharply truncated foliation, small pegmatite dikes, dilational features and the rotated xenolith are strong evidence for the intrusive nature of the pegmatite/aplite.

Contact relationships between the Zoroaster Gneiss and the pegmatite/aplite dikes show that at least some of the pegmatite formed by replacement of the gneiss. These contacts vary from extremely sharp to gradational with the gneissosity penetrating the margins of the dikes (see Figure 12). Many dikes are developed along unopened fractures in the gneiss and do not dilate the gneiss.

This observation also implies that the replacement media was a fluid rather than a magma. Further evidence for crystallization from a fluid are the numerous, pure quartz centered dikes. In a granitic system it is impossible to crystallize pure quartz from a magma unless the parent for the magma was pure quartz (Bowen, 1928). Some dikes are only one cm thick and tens of meters in length. It would seem that the viscosity of a silica-rich magma would preclude such dimensions. Many dikes in Zoroaster Canyon cut other pegmatite dikes with no dilational effect.

Contrary to this evidence, it should be noted that the amphibolite at Cremation Creek appears to have been forcibly shouldered aside. If this interpretation is correct, then a intrusive origin is likely for this group of dikes.

The three, tourmaline-bearing, pegmatite dikes observed in the Clear Creek drainage show little or no resemblance to those in the Zoroaster Canyon-Cremation Creek area.

Aplite and pegmatite are composed primarily of quartz, plagioclase, and microcline with lesser amounts of biotite and muscovite. Modal analyses of aplite samples show that these rocks fall near the thermal trough and are similar to the Zoroaster Gneiss in composition (Figure 13). The average aplite is composed of 40% plagioclase, 40% quartz, 17% microcline, and 3% biotite and muscovite. In hand specimen there appears to be considerably more microcline because hematite stains both plagioclase and microcline pink.

In pegmatites, most crystals range from 2 to 15 mm, but some feldspar crystals 30 cm in diameter have been observed. These very large crystals are additional evidence for crystallization from a fluid.

Garnets are common accessory minerals in aplites and pegmatites. These occur in sinuous layers or as individual layers. Other accessory minerals are apatite, tourmaline and opaques.

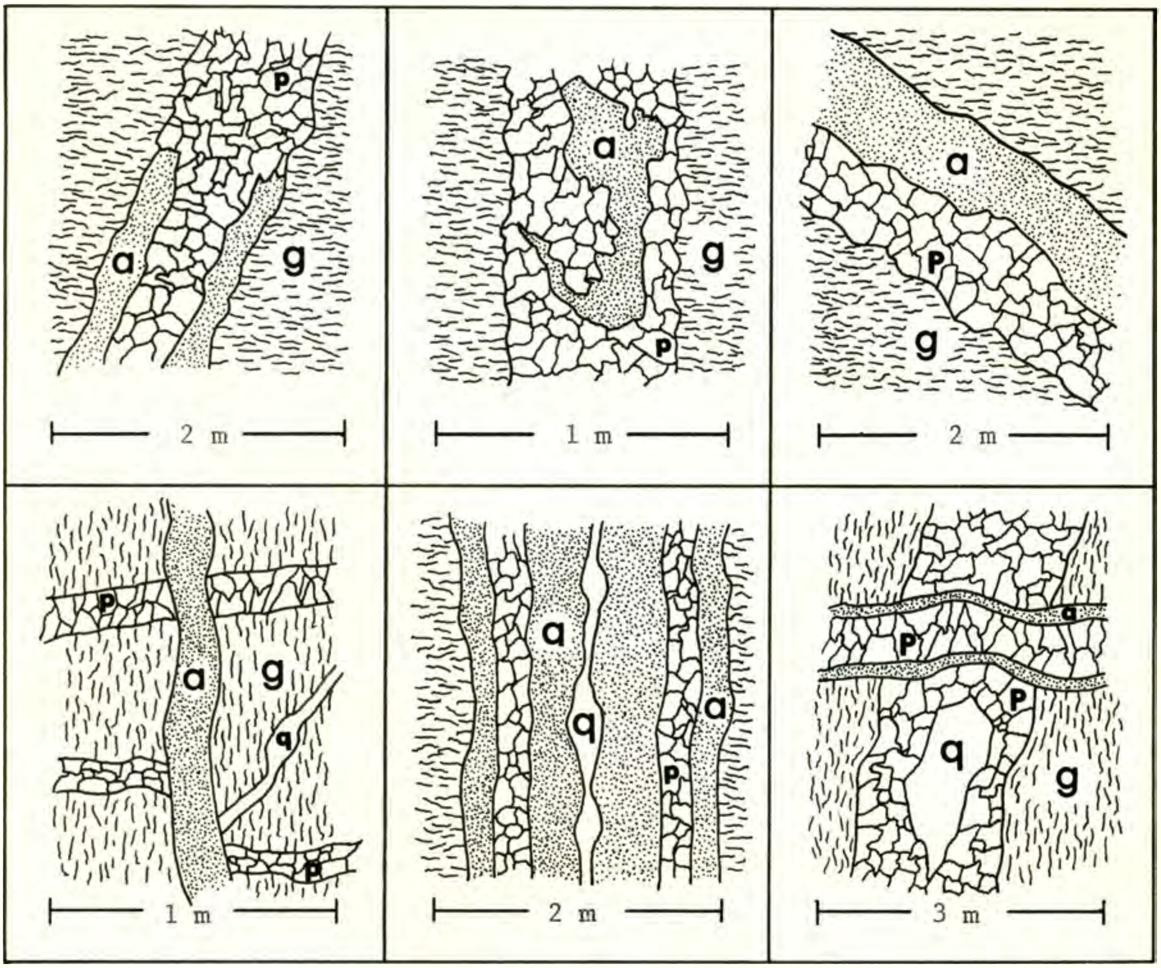

Figure 15. Some relationships between gneiss (g), pegmatite (p), aplite (a), and quartz (q) in dikes and sills from the Zoroaster monadnock and Cremation Creek.

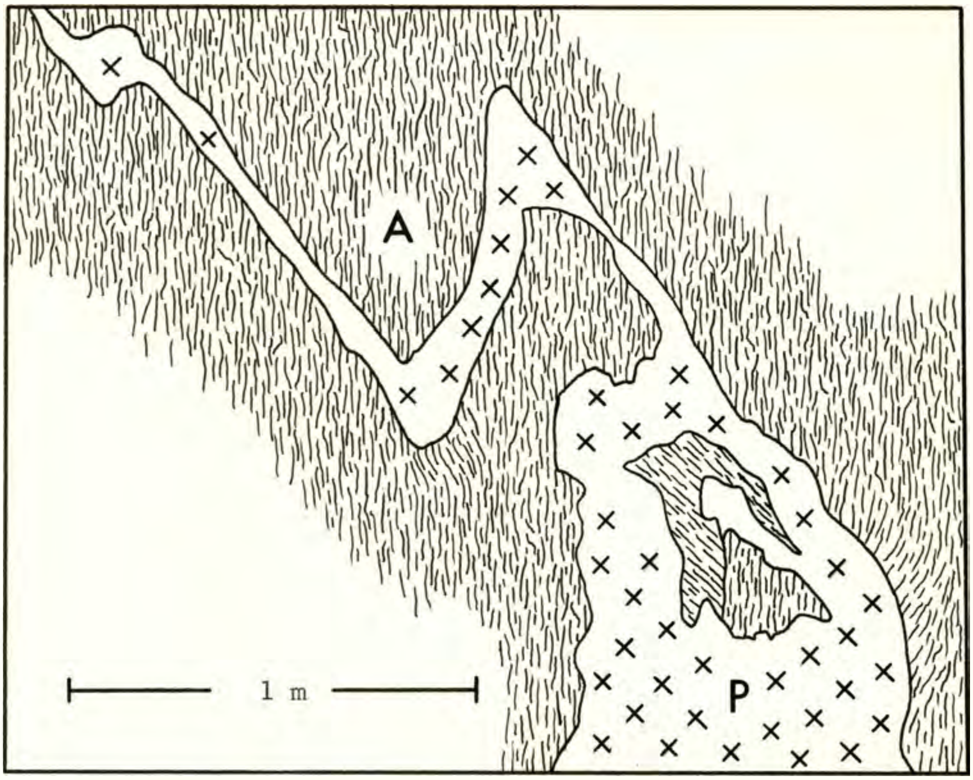

Figure 16. Pegmatite dike (P) in amphibolite (A) from Cremation Creek. Note the rotated xenolith within the pegmatite. The geometry of this dike could have resulted from post injection shear folding (quasi-flexural folding of Boyce, 1972), or by injection along a curved fracture. In either case, considerable replacement of the host amphibolite is indicated.

STRUCTURES

Lithologic Layering

Lithologic layering in the Vishnu Schist is composed of the micaceous schists, metamorphosed calc-silicate rocks, quartzites, and amphibolites described in the preceding sections. These layers are vertically oriented and strike northeast. Individual layers are from twenty centimeters to tens of meters in thickness and they can be traced for hundreds of meters along strike. Longitudinally discontinuous layers have intertonguing relationships with contiguous layers.

Lithologic layering is a pervasive element in the Vishnu Schist; it is interrupted only in the mobilized zones of chlorite-garnet schist and by quartzo-feldspathic veins. The mobilized zones contort the lithologic layering into tight disharmonic folds. Quartzo-feldspathic veins run parallel with the lithologic layering and display pinch and swell structure, and boudinage.

The lithologic layering will be called S_o.

Schistosity

The dominant structural element of the Vishnu Schist and the Zoroaster Gneiss is a well developed vertical schistosity (Figure 17). The schistosity mostly strikes northeast (Figure 18) and is perfectly concordant with the lithologic layering. Figure 19 shows a typical view of S_1 and So. It is penetrative on a mesoscopic scale with the exception of the weakly foliated amphibolite layers. In thin section, it is generally penetrative but many sections show other planar structure, or intense deformation with little or no planar structure. This foliation will be called S_1.

A second foliation has been noted in thin section. This foliation, which will be called S_2, is defined by the parallel alignment of late biotite cross-micas or strain-slip cleavage traces (see Figure 4). Vertically oriented strain-slip cleavage has been observed in the field by M.D. Clark (personal communication) but it is not known whether this is the pervasive orientation. In thin section S_2 cuts S_1 at an angle of 30 to 40°.

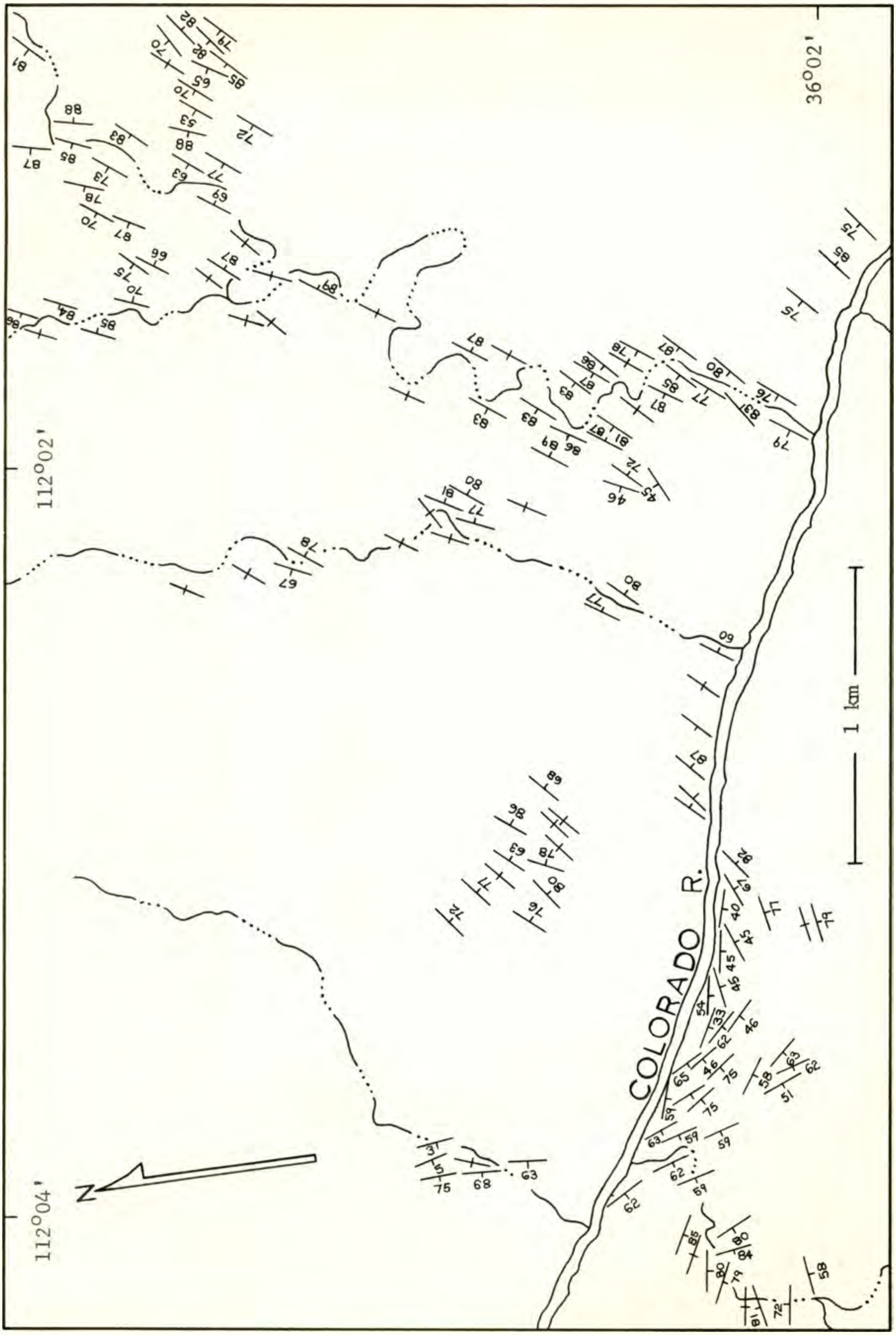

Figure 17. A map of the attitudes of S_1.

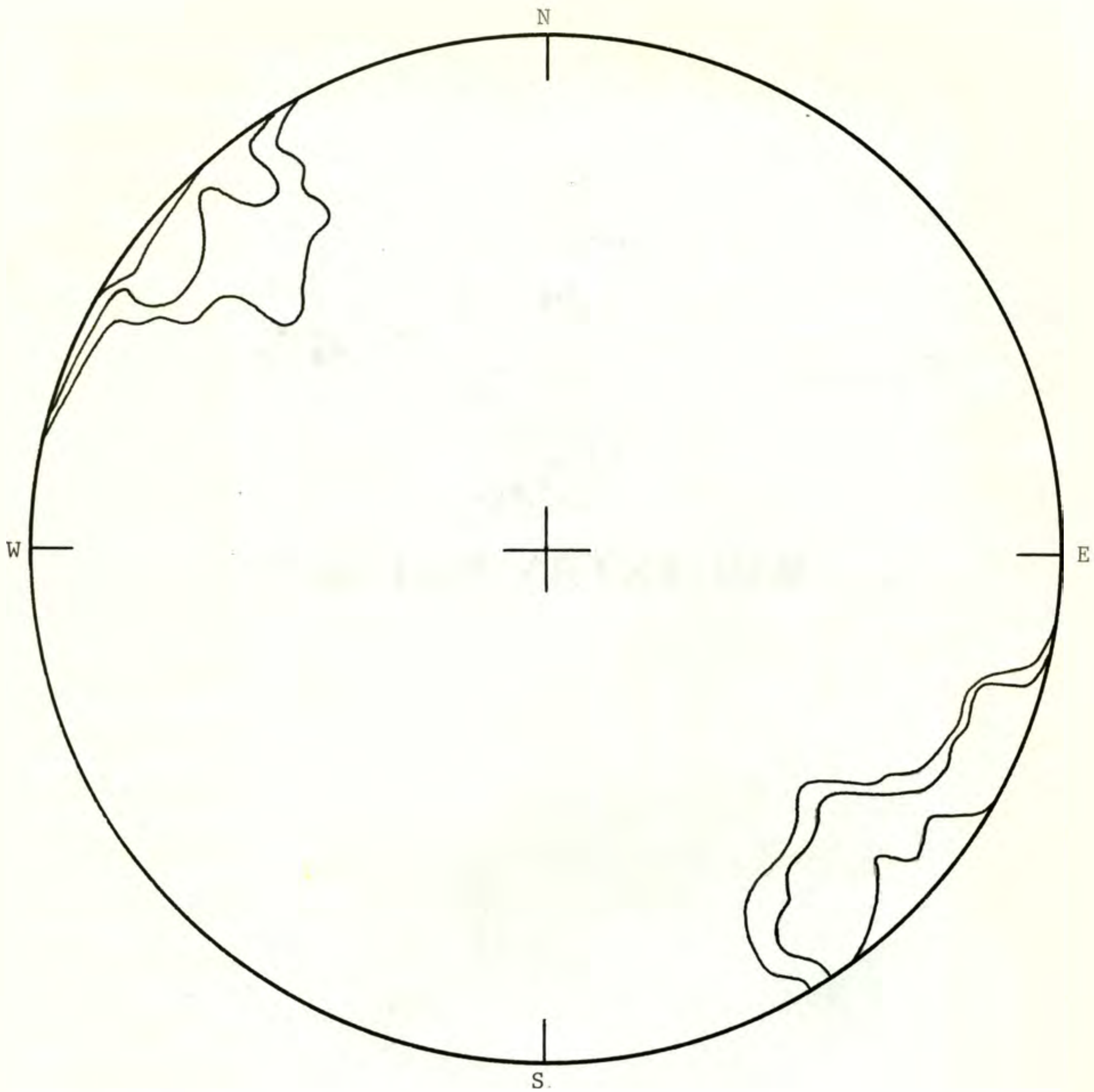

Figure 18. Equal area, lower hemisphere projection of 112 poles to the foliation in Zoroaster Canyon and the Clear Creek area. Contours are at 2, 4, and 8 percent of a one-percent area.

0.5 km

Figure 19. View looking northeast into Clear Creek canyon showing vertically oriented schistosity and lithologic layering.

Lineations

A crenulation lineation was observed 200 m east of the mouth of Zoroaster Canyon. The orientation is N66E, 68E. Similar lineations have been reported by Brown and these cut a vertical hornblende lineation (personal communication, 1972). This is further evidence for two generations of small scale structures but more detailed work is necessary to work out all the deformational relationships.

A lineation of horizontal boudin axes trending parallel with S_1 is present in lower Clear Creek Canyon. Figure 20 shows typical boudinage.

Microfolding

Crenulations, kink bands and chevron folds are spectacularly developed in the Vishnu Schist. Tight crenulations with axial planes at high angles to S_1 have been observed in several thin sections. Crenulations in a few samples are breached by axial thrusts which define a non-penetrative, strain-slip cleavage (Figure 21).

Kink bands within individual biotites and, less commonly in chlorites and muscovites, occur as intermeshing blades or as chevron pairs. Conjugate kink bands are developed in a few muscovites. Kink banding is particularly well developed in post-tectonic, biotite porphyroblasts.

Chevron folds with vertical axial planes and axes parallel to S_1 have been found in conjunction with mesoscopic F_2 folds.

The kink bands, crenulations and other deformation textures such as undulose extinction in quartz and plagioclase, strained quartz showing a small 2V, and deformation twins in plagioclase, are good evidence of late deformation of the Vishnu Schist.

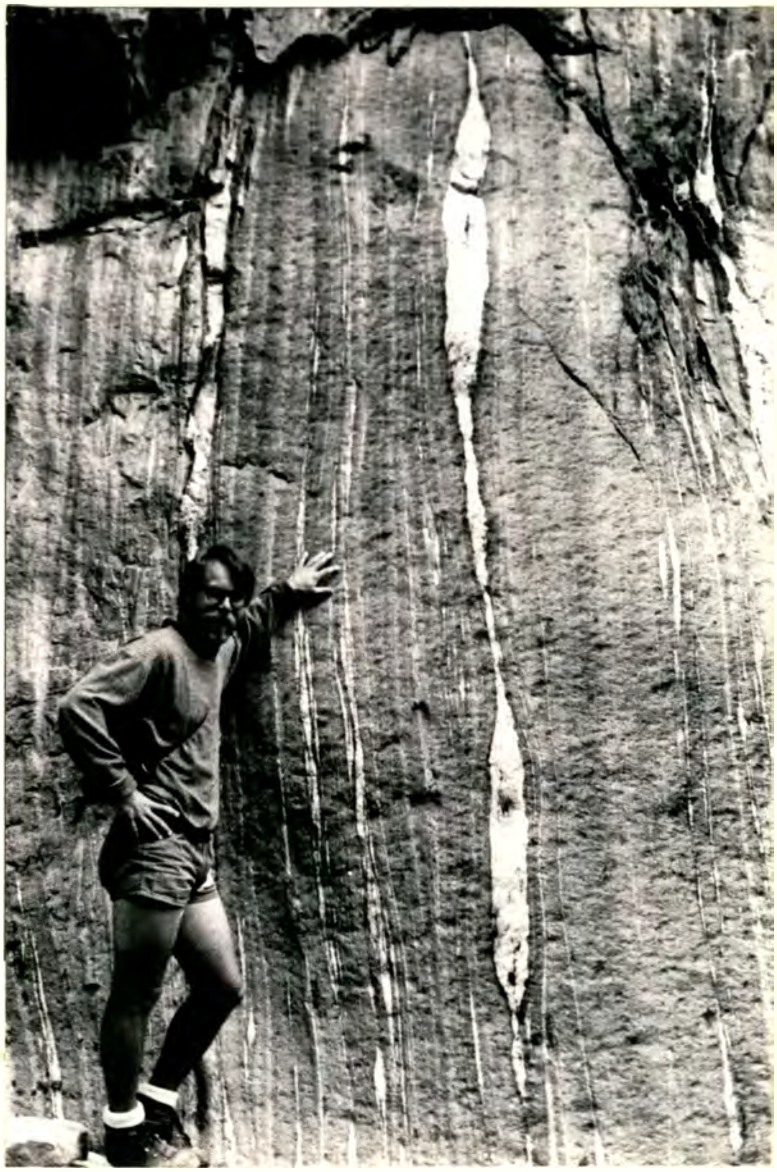

1 m

Figure 20. Boudinage in quartzo-feldspathic veins from lower Clear Creek canyon.

2 mm

Figure 21. Photomicrograph of non-penetrative strain-slip cleavage from sample 46-V11.

Mesoscopic Folding

Mesoscopic folds which bend S_1 are prevalent throughout the study area, but only one fold with axial plane schistosity has been observed.

The fold with axial plane schistosity is located twenty meters west of the mouth of Clear Creek (Figure 22). It has a vertical axis and an amplitude of 2.5 meters. The fold style is similar but the limbs show a peculiar branching characteristic. This fold may correspond to the "obscure earlier episode of folding" reported by Ragan (1970). It will be referred to as F_1.

The predominant group of folds in the study area bend S_1 around horizontal axes and have vertical axial planes which strike northeast, parallel to the general trend of S_1. In many cases the axes have been refolded and their original horizontal attitude can only be inferred. Individual folds where the axes plunge steeply northeast and southwest at opposite ends have been observed. These are nearly horizontal in the middle. All of these folds are classified F_2. There are concentrations of F_2 folds with near vertical and near horizontal axes, but their axes may plunge at any angle (Figure 23). Folds of this type have been observed at Bright Angel Creek (Boyce, 1972). Figure 24 shows the attitude of F_2 folds at Bright Angel Creek. Figure 25 is a map of the distribution of F_2.

Similar folds are the most common style of F_2 folding and flexure flow is the apparent mechanism of yielding (Figure 26). Disharmonically folded quartzo-feldspathic veins occur within individual similar folds. Many folds with mixed similar and concentric styles have been observed in subordinate competent layers (Figure 27).

All the F_2 folds with horizontal axes in the Clear Creek drainage are symmetrical, but most F_2 folds in Zoroaster Canyon are asymmetrical. Here the west limb is structurally higher. The distribution of F_2 folds is shown in Figure 25.

Superimposed on F_2, are folds with vertical axial planes and subhorizontal axes trending northwest. These folds, which are only observed in conjunction with F_2 folds, are thought to give F_2 axes their variable plunge. Evidence for this includes F_2 axes which are folded as much as 90^o and the relatively uniform distribution of all F_2 axes around a hypothetical, northwest trending axis. These folds could have formed concomitantly with F_2, or they may be separate generations. Boyce (1972) has recognized folds of this type in the Bright Angel Creek area. He has classified them as open flexural folds. These folds have measured axes of two to seven meters. They are tentatively classified F_3.

The schistosity, F_2, and F_3 folds are refolded by gentle warps with horizontal axes and axial planes. These refolds trend parallel with S_1. They will be referred to as F_4. Figure 28 shows F_4 superimposed on F_2 and Figure 29 shows the relationship of F_2 and F_3. Whether or not these represent three separate generations is a matter of conjecture and further study in this area is called for.

Minor ptygmatic and other disharmonic folds are present in the mobilized zones of chlorite-garnet schist in upper Clear Creek. Intrafoliation folds occur with vertical necking and boudinage in the quartzo-feldspathic veins or lower Clear Creek (Figure 30). The boudin lines are roughly horizontal.

Figure 22. Fold with axial plane schistosity (F_1) from Clear Creek. The fold axis is vertical and the scale is 16 cm. long.

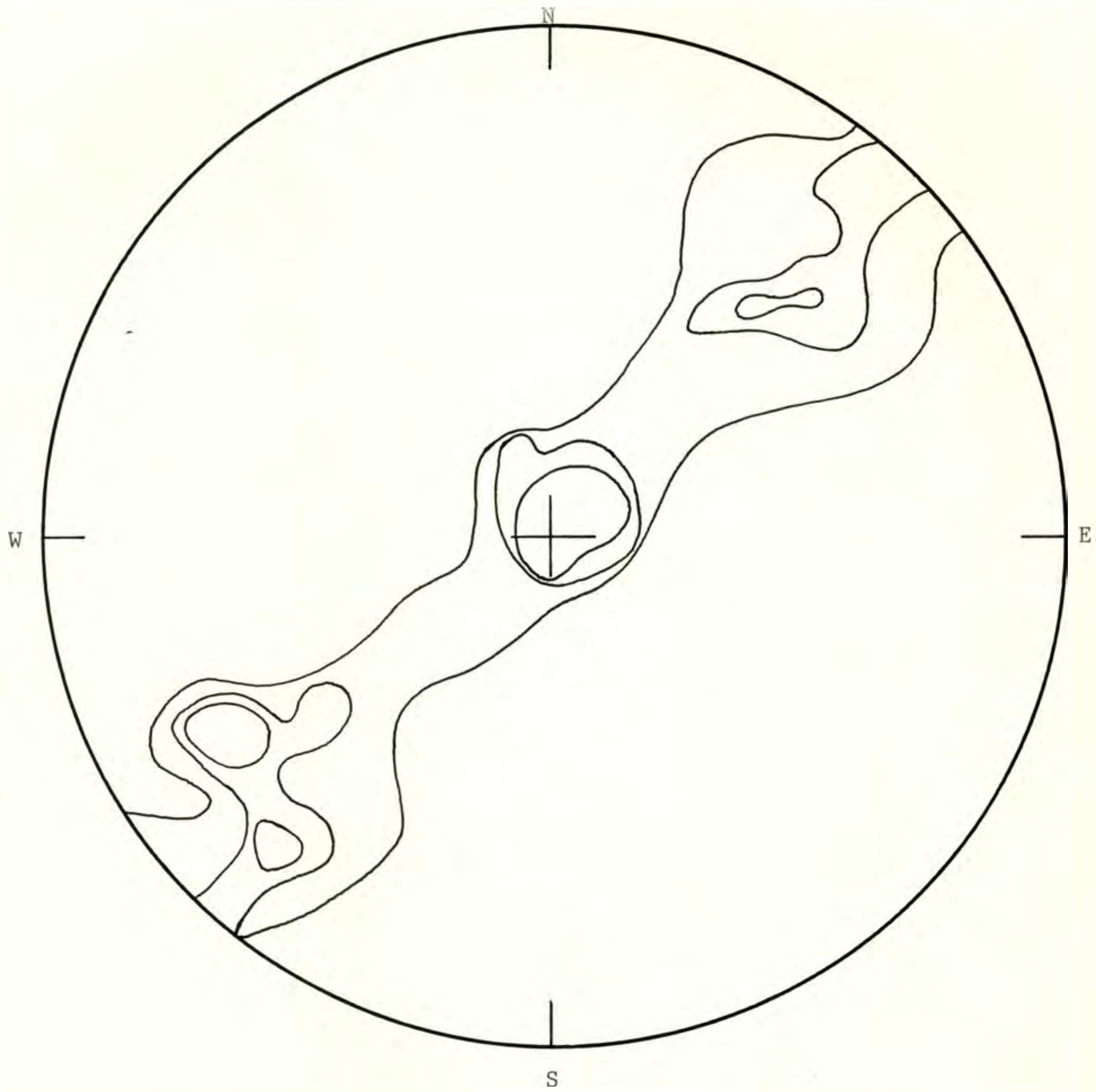

Figure 23. Equal-area, lower hemisphere projection of 39 fold axes from the vicinity of Clear Creek. Contours are 2, 6, and 9 percent of a one percent area. Note that these axes are symmetrically distributed around a horizontal, northwest trending axis.

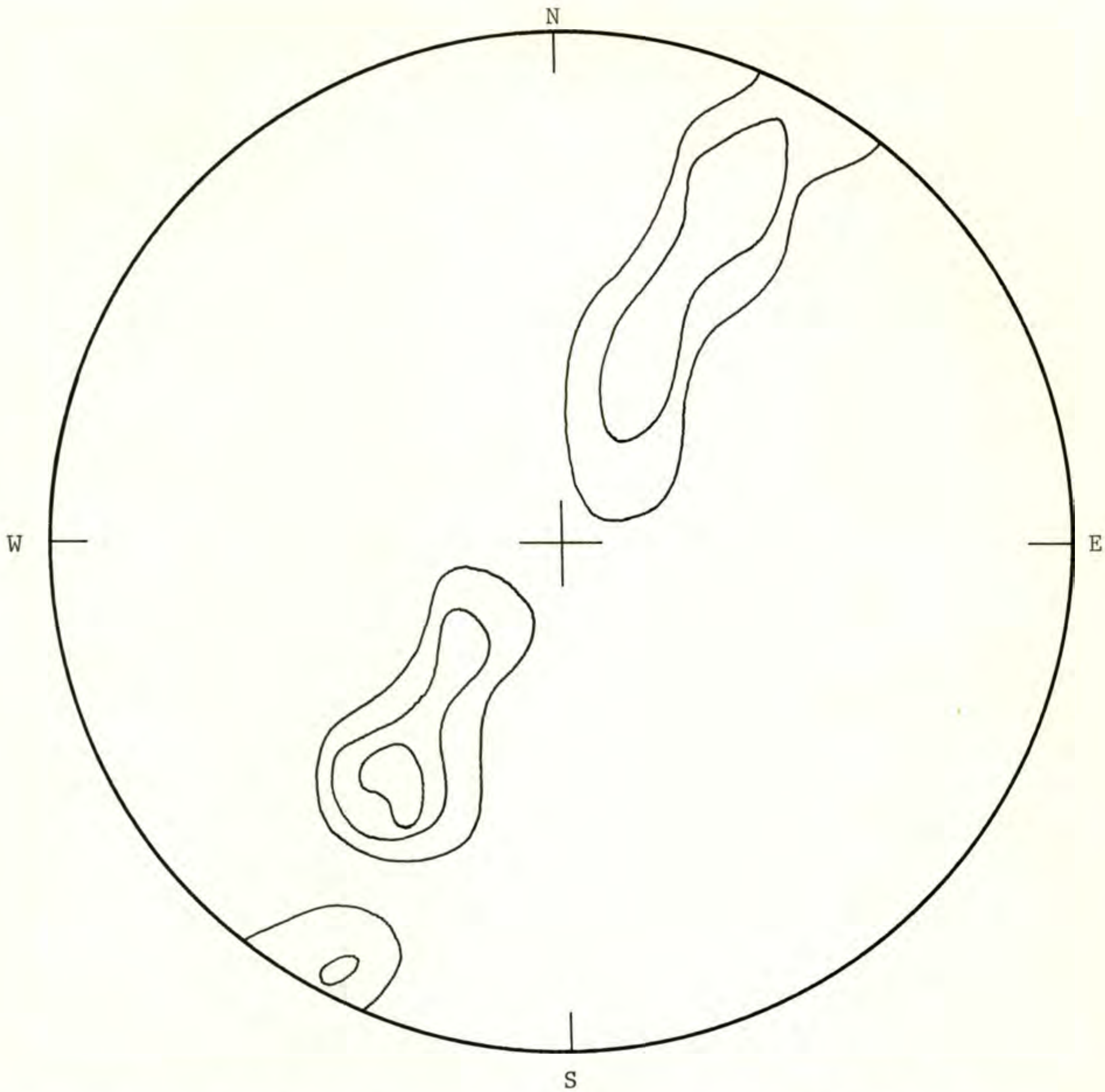

Figure 24. Equal-area, lower hemisphere projection of 23 fold axes of concentric folds from Bright Angel Canyon (after Boyce, 1972). Contours are at 2, 9, and 16 percent of a one percent area. These folds correspond to the F_2 folds of the present study.

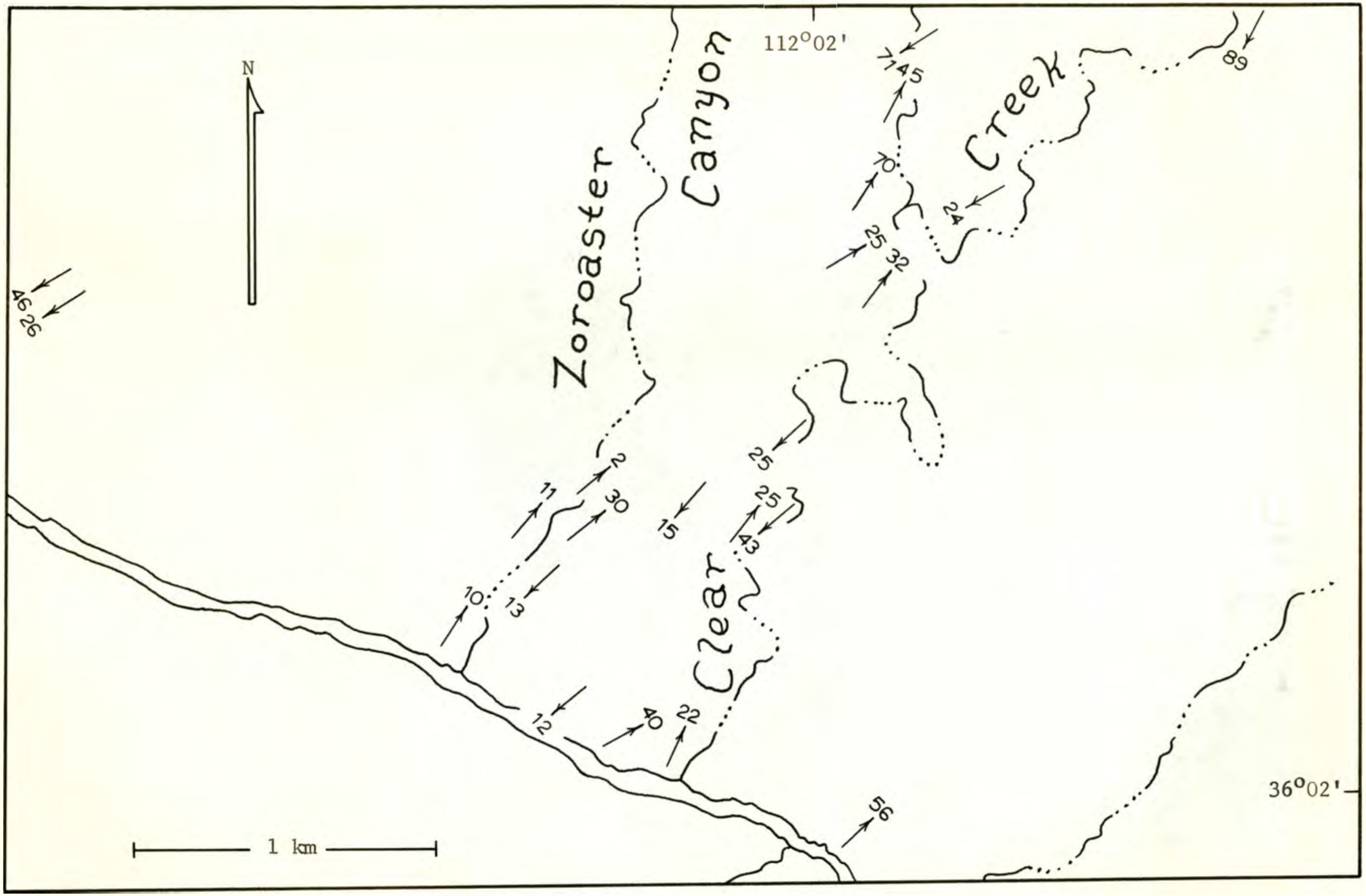

Figure 25. The distribution of some F_2 folds.

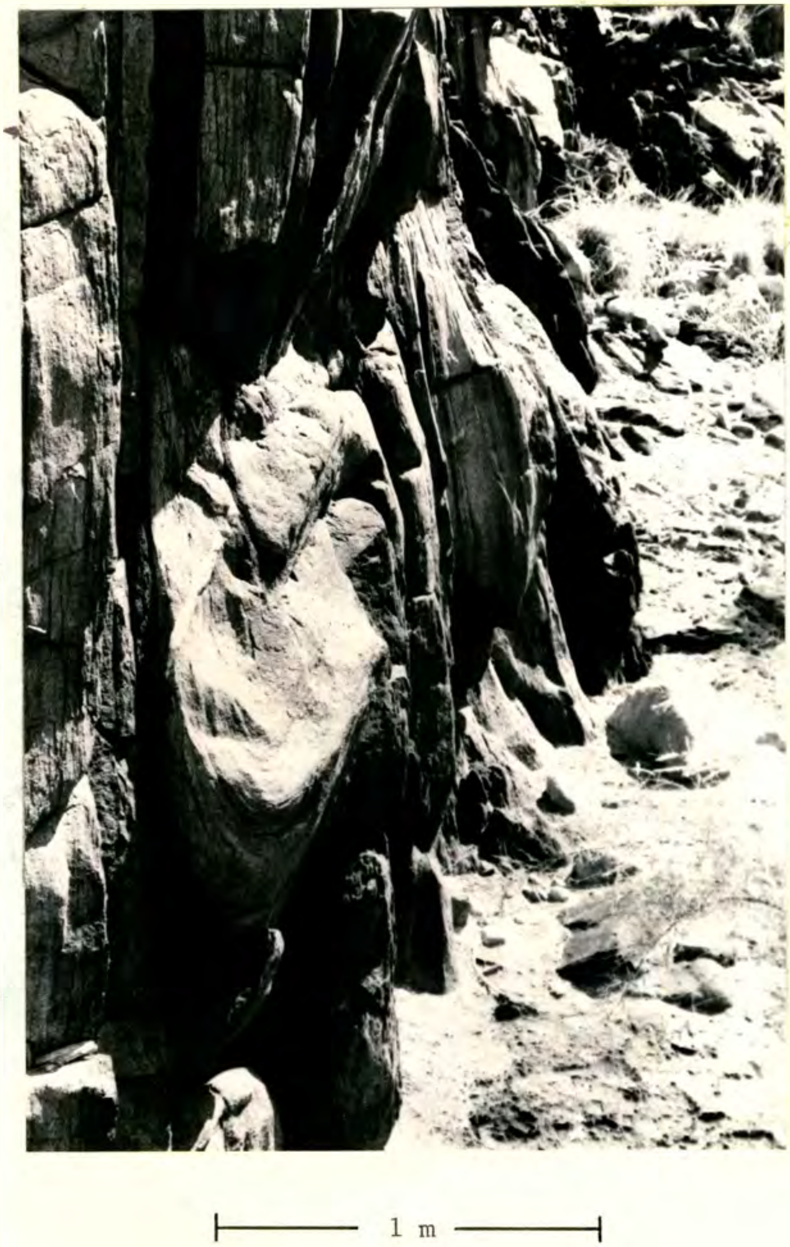

Figure 26. Similar style F_2 fold from Clear Creek. Axis is near horizontal.

0.5 m

Figure 27. F_2 fold showing both concentric and similar styles from Clear Creek. The axis is horizontal.

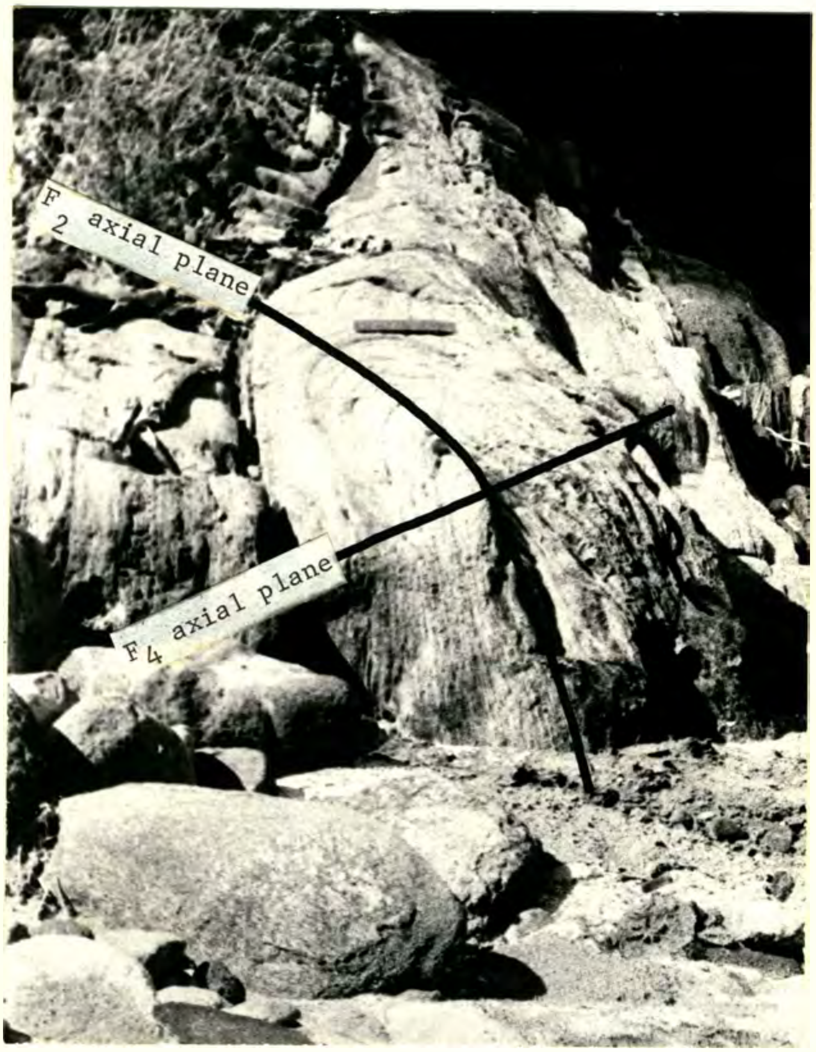

Figure 28. Relationship of F_2 and F_4 folds in Clear Creek. The scale is 16 cm.

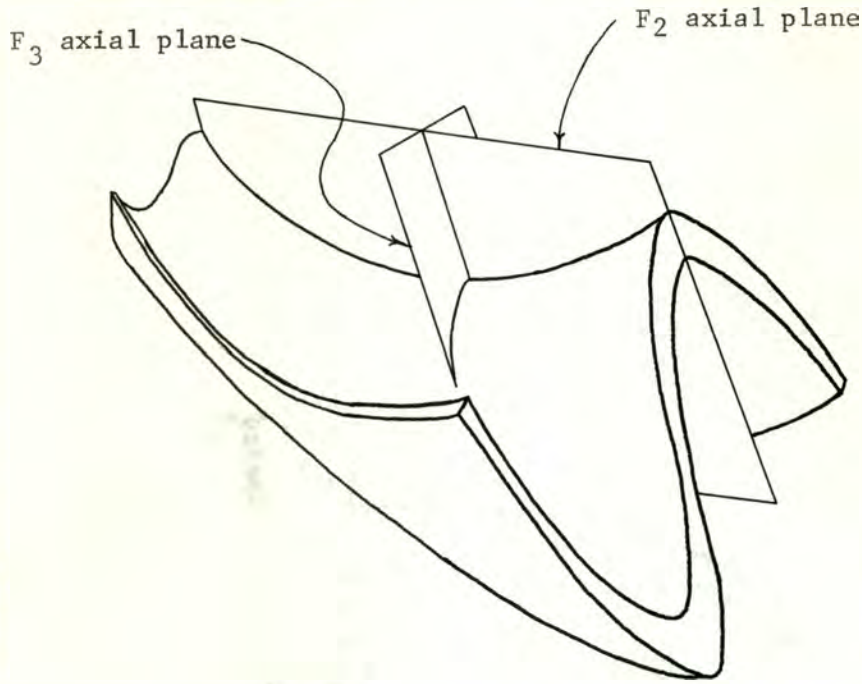

Figure 29. The relationship between F_2 and F_3 folds.

├──── 64 cm ────┤

Figure 30. Intrafoliation folds and boudinage in quartzo-feldspathic veins from lower Clear Creek canyon.

Macroscopic Folding

Macroscopic folding in the study area consists of an anticlinal or dome structure and its parasitic folds. The existence of macroscopic isoclinal folds was hypothesized by Maxson (1968), but little evidence of such folding was observed in the study area.

The form surface of the anticlinal or dome structure is defined by the map of the attitudes of S_1 (see Figure 17). Jointing and amphibolite sills parallel to S_1 help delineate the structure when viewed from one side of the Colorado River to the other. This fold bends both the amphibolite and the Zoroaster Gneiss east of Cremation Creek.

Poles to the foliation were used to construct a π-circle for a domain south of the Colorado River and east of Cremation Creek where the structure is most accessible (Figure 31). This analysis yields a best-fit fold axis attitude of S72W59 for this domain of the structure.

Unfortunately, many crucial outcrops, especially those on the north side of the Colorado River, were inaccessible. Consequently the exact nature of this structure remains unknown.

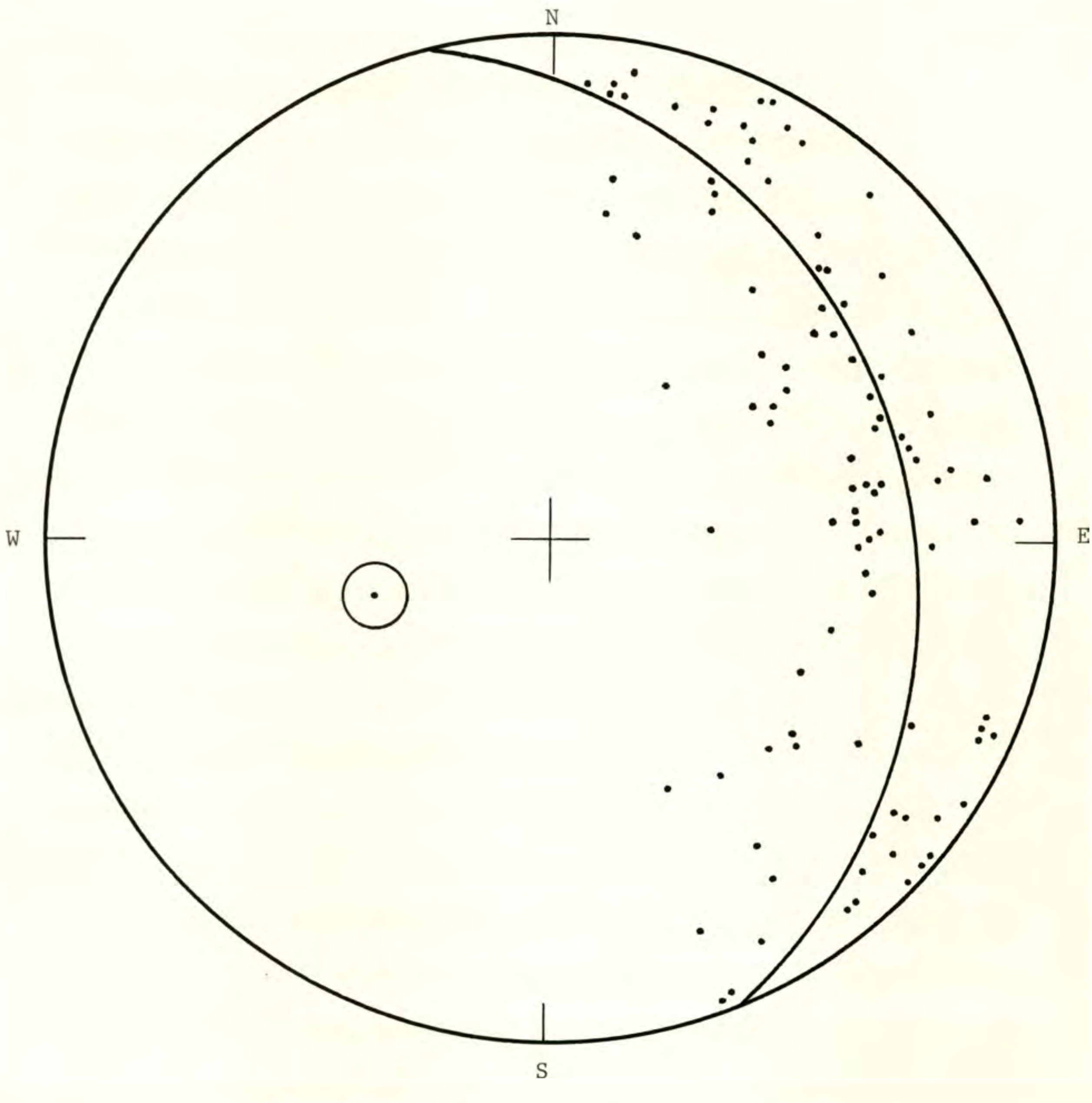

Figure 31. Equal-area, lower hemisphere projection of 100 poles to foliation taken west of Zoroaster Canyon. The curve is a best fit π-circle for a macroscopic fold defined by these poles. The circled point is the calculated fold axis which trends S72W59.

Interpretation of Macroscopic Structures

The macroscopic structure described in the preceding section might be a noncyclindrical anticline, a mantled gneiss dome, or a dome caused by the injection of late pegmatite. The delicate nature of structures at the Vishnu-Schist Zoroaster Gneiss contact was previously mentioned as evidence against a gneiss dome. If either of the doming mechanisms were responsible for the macroscopic folding, the limbs of the mesoscopic folds should double back on themselves forming reverse drag folds. These have not been observed. The sense of vergence of most F_2 folds in Zoroaster Canyon suggests that an anticline is present to the west. The exact nature of this structure can only be established by further study.

Other possible macroscopic structures are isoclinal folds suggested by the concordancy of S_0 and S_1. Maxson and Campbell felt that isoclinal folds are present in the Grand Canyon and that these have horizontal axes. Ragan and Sheridan (1970) suggest that the hypothesized isoclinal folds must have vertical axes. Although few structures were observed in the study area which could be used to test either hypothesis, the F_1 fold and the vertical lineations seem to support Ragan's model.

Time Relationships of Geologic Events

The order of deposition and intrusion of the various rock types found in the study area from oldest to youngest is: Vishnu deposition, emplacement of quartzo-feldspathic veins, Zoroaster intrusion, emplacement of amphibolite sills within the gneiss, and pegmatite/aplite intrusion. Amphibolite bodies at Clear Creek and Cremation Creek may have been emplaced synchronously with the amphibolite sills in the gneiss, or the gneiss may have intruded the amphibolite. The former hypothesis seem preferable.

Metamorphism and deformation probably spanned a long time period. Metamorphism could have started any time after deposition of the Vishnu sediments deposition. Metamorphism must have been active after the amphibolite sills in the gneiss were emplaced. Retrogressive metamorphism may have outlasted pegmatite/aplite intrusion. Biotites in the pegmatite-amphibolite contact alteration zone are replaced by a retrogressive chlorite-potash feldspar assemblage.

The writer believes that deformation was active prior to the emplacement of the Zoroaster magma. The Zoroaster magma is thought to be intruded along a plane of schistosity rather than a relict bedding plane, but more careful observation will be required to substantiate this.

These time relationships are summarized in Figure 32.

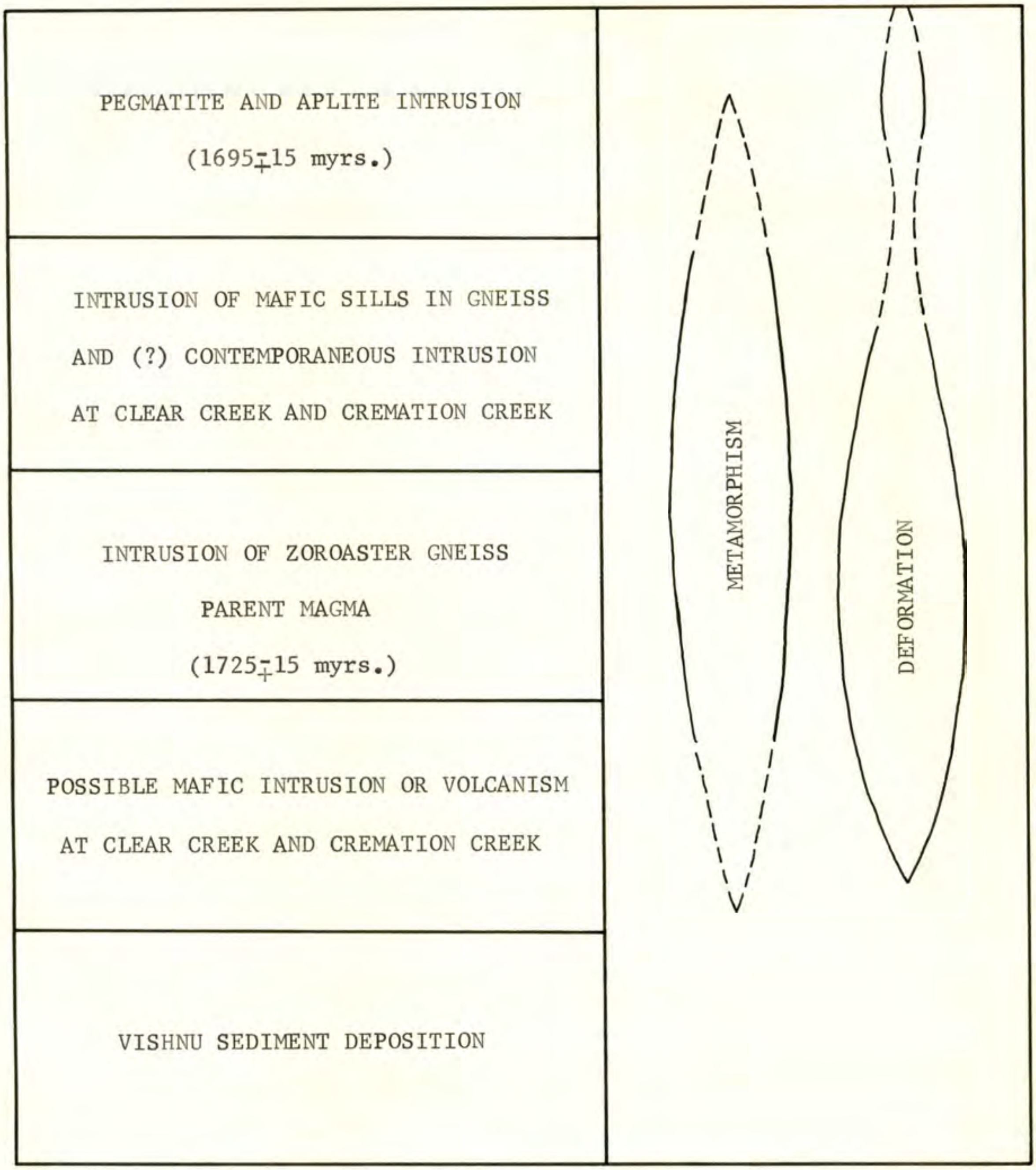

Figure 32. Inferred chronologic scheme for the emplacement of rock units, metamorphism, and deformation. Dates are from Pasteels and Silver (1965).

REFERENCES CITED

Albee, A.L., 1965, Distribution of Fe, Mg, and Mn between garnet and biotite in natural mineral assemblages: Jour. Geology, v. 73, p. 155-164.

__________ 1968, Metamorphic zones in northern Vermont in Studies of Appalachian Geology: New York, Interscience, p. 329-341.

__________ 1972, Metamorphism of pelitic schists: Reaction relations of chloritoid and staurolite: Geol. Soc. America Bull., v. 83, p. 3249-3268.

Atherton, M.P., 1968, The variation in garnet biotite and chlorite composition in medium grade pelitic rocks from the Dalradian, Scotland: Contr. Mineral. and Petrol., v. 18, p. 347-371.

Bailey, E.H., and Stevens, R.E., 1960, Selective staining of K-feldspar and plagioclase on rock slabs and in thin section: Am. Mineralogist, v. 45, p. 1020-1025.

Bowen, N.L., 1928, The evolution of the igneous rocks: New York, Dover, 334 p.

Boyce, M.J., 1972, Structure and petrology of the older Precambrian crystalline rocks, Bright Angel Canyon, Arizona: unpublished M.S. thesis, Univ. of Northern Arizona, Flagstaff, Arizona.

Brown, E.H., 1967, The greenschist facies in part of eastern Otago, New Zealand: Contr. Mineral. and Petrol., v. 14, p. 347-371.

__________ 1969, Some zoned garnets from the greenschist facies: Am. Mineralogist, v. 54, p. 1662-1677.

Campbell, I., 1936, On the occurrence of sillimanite and staurolite in the Grand Canyon: Grand Canyon Natural History Bull., v. 5, p. 17-22.

__________ and Maxson, J.H., 1933, Some observations on the Archean metamorphics of the Grand Canyon: (U.S.) Natl. Acad. Sci. Proc., v. 19, p. 806-809.

__________ 1934, Geological studies of the Archean rocks at Grand Canyon: Carnegie Inst. Washington Year Book, v. 34, p. 323-326.

__________ 1936, Geological studies of the Archean rocks at Grand Canyon: Carnegie Inst. Washington Year Book, v. 35, p. 330-331.

Carmichael, D.M., 1970, Intersecting isograds in the Whetstone Lake area Ontario: Jour. Petrology, v. 11, p. 147-181.

Chakraborty, K.R., and Sen, S.K., 1967, Regional metamorphism of pelitic rocks around Kandra, Singhbhum, Bihar: Contr. Mineral. and Petrol., v. 16, p. 210-232.

Chayes, F., 1956, Petrographic modal analysis: New York, John Wiley and Sons, 113 p.

Chinner, G.A., 1961, The origin of sillimanite at Glen Clova, Angus, Scotland: Jour. Petrology, v. 2, p. 312-323.

Damon, P.E., 1968, K-Ar dating of igneous and metamorphic rocks with application to the Basin ranges of Arizona and Sonora, in Radiometric dating for geologists: New York, Interscience, p. 1-71.

Francis, G.H., 1956, Facies boundaries in pelites at the middle grades of regional metamorphism: Geol. Mag., v. 93, p. 353-368.

Ganguly, J., 1968, Analysis of the stabilities of chloritoid and staurolite and some equilibria in the system $FeO-Al_2O_3-SiO_2m-H_2O-O_2$: Am. Jour. Sc., v. 266, p. 277-298.

__________ 1969, Chloritoid stability and related parageneses: Theory, experiments, and application: Am. Jour. Sci., v. 267, p. 910-944.

__________ 1972, Staurolite stability and related parageneses: Theory, experiments, and application: Jour. Petrology, v. 13, p. 335-368.

Heinrich, E.W., 1965, Microscopic identification of minerals: New York, McGraw Hill Book Co., 414 p.

Heitenan, A., 1969, Distribution of Fe and Mg between garnet, staurolite, and biotite in aluminum-rich schist in various metamorphic zones north of the Idaho Batholith: Am. Jour. Sci., v. 207, p. 422-456.

Hollister, L.S., 1966, Garnet zoning: An interpretation based on the Rayliegh fractionation model: Science, v. 207, p. 423-456.

Laniz, R.V., Stevens, R.E., and Norman, M.B., 1964, Plagioclase feldspar staining with F.D. and C. red no. 2: U.S. Geol. Survey Prof. Paper 501-13, p. B152-B153.

Luth, W.C., Jahns, R.H., and Tuttle, O.F., 1964, The granite system at pressures of 4 to 10 kilobars: Jour. Geophysical Research, v. 69, p. 759-773.

Lyons, J.B., and Morse, S.A., 1970, Mg/Fe partitioning in garnet and biotite from some granitic, pelitic, and calcic rocks: Am. Mineralogist, v. 55, p. 231-245.

Maxson, J.H., 1961 (revised 1968), Geologic map of the Bright Angel Quadrangle: Grand Canyon Natural History Assoc.

__________ 1967, Preliminary Geologic Map of Grand Canyon National Park, Eastern section: Grand Canyon Natural History Assoc.

Noble, L.F., and Hunter, J.F., 1916, A reconnaissance of the Archean Complex of Granite Gorge, Grand Canyon, Arizona: U.S. Geol. Survey Prof. Paper 98-I, p. 95-113.

Pasteels, P., and Silver, L.T., 1965, Geochronologic investigations in the crystalline rocks of the Grand Canyon, Arizona (abs): Geol. Soc. Am. Program, p. 122.

Ragan, D.M., and Sheridan, M.F., 1970, Archean rocks of the Grand Canyon, Arizona (abs): Geol. Soc. Am. Program, p. 132.

Slemmons, D.B., 1962, Determination of volcanic and plutonic plagioclases using a three or four-axis universal stage: Geol. Soc. Am. Special Paper 69, 64 p.

Spry, A., 1969, Metamorphic textures: New York, Pergamon, 350 p.

Stuart, B.A., 1962, The composition of garnets from pelitic schists in relation to grade of regional metamorphism: Jour. Petrology, v. 3, p. 181-191.

Thompson, J.B., and Norton, S.A., 1968, Paleozoic regional metamorphism in New England and adjacent areas, in Studies of Appalachian geology: New York, Interscience, p. 319-327.

Tozer, C.F., 1955, Sillimanite in the Glen District, Co., Donegal: Geol. Mag., v. 92, p. 310-320.

Troger, W.E., 1959, Optische bestimmung der gesteinsbildenden Minerale: Stuttgart, E. Schweizerbart'sche Verlagsbuchhandlung, 147 p.

Walcott, C.D., 1894, Precambrian igneous rocks of the Unkar terrain, Grand Canyon, Arizona: U.S. Geol. Survey Ann. Rept., v. 14, p. 497-524.

Weill, D.F., and Kudo, A.M., 1968, Initial melting in alkali feldspar-plagioclase-quartz systems: Geol. Mag., v. 105, p. 325-337.

Williams, H., Turner, F.J., and Gilbert, C.M., 1954, Petrography: An introduction to the study of rocks in thin section: W.H. Freeman and Co., San Francisco, 406 p.

Winkler, H.G.F., 1967, Petrogeneses of metamorphic rocks: Springer-Verlag, 220 p.

APPENDIX A

MINERAL ASSEMBLAGES OBSERVED IN THIN SECTION

Sample	Rock type	Plagioclase	K-Feldspar	Quartz	Biotite	Muscovite	Chlorite	Garnet	Staurolite	Sillimanite	Hornblende	Actinolite	Calcite	Epidote	Sphene	Tourmaline	Apatite	Zircon
46-V2	calcsilicate	x		x				x				x	x		x			
46-V8	mica schist	x		x	x	x	x	x	x									
46-V9	amphibolite	x									x		x		x			
46-V11	mica schist	x		x	x	x	x	x										x
46-12	gneiss	x	x	x		x											x	x
46-13	gneiss	x	x	x	x	x											x	
46-14	aplite	x	x	x	x	x												
46-16	aplite	x	x	x	x	x		x										
46-18	aplite	x	x	x	x	x												
46-19	aplite	x	x	x	x	x	x											
46-20a	mica schist	x		x	x	x								x	?		x	
46-20b	gneiss	x	x	x	x	x											x	
46-27	gneiss	x	x	x	x	x												
46-29	gneiss	x	x	x	x	x											x	
46-30	gneiss	x	x	x	x	x	x								x		x	
46-31	mica schist	x		x	x	x	x											x
46-34	mica schist	x		x	x	x											x	x
46-35	gneiss	x	x	x	x	x								?				
46-36	gneiss	x	x	x	x									?			x	
46-40	amphibolite	x		x	x		x				x				x		x	
46-41	amphibolite	x			x						x				x		x	
46-42	aplite	x	x	x		x												
46-45	gneiss	x	x	x	x	x	x											
46-46	gneiss	x	x	x	x		x											x
46-47	amphibolite	x		x	x						x			x	?		x	
46-48	amphibolite	x		x	x						x			x			x	
46-53	mica schist	x		x			x							x	x		x	
46-54	gneiss	x	x	x	x	x												x
46-57	gneiss	x	x	x	x	x	x											x
46-62	aplite	x	x	x		x											x	
46-65	gneiss	x	x	x	x	x											x	x
46-70	aplite	x	x	x		x												
46-74	gneiss	x	x	x	x	x								?				
46-75	pegmatite	x	x	x		x												
46-77	aplite	x	x	x		x											x	
46-78	aplite	x	x	x	x	x										x		x

All assemblages include opaques.

Sample	Rock Type	Plagioclase	K-Feldspar	Quartz	Biotite	Muscovite	Chlorite	Garnet	Staurolite	Sillimanite	Hornblende	Actinolite	Calcite	Epidote	Sphene	Tourmaline	Apatite	Zircon
46-79	gneiss	x	x	x	x	x												x
46-80	late granitic	x	x	x	x	x												
46-82	late granitic	x	x	x	x	x		x									x	
46-83	aplite	x	x	x	x	x												
46-85	gneiss	x	x	x	x	x												
46-90	amphibolite	x									x				x			x
46-93	amphibolite	x			x		x				x						x	
46-94	amphibolite	x			x						x			x	?			
46-97	mica schist	x		x	x	x	x	x	x	x						x		x
46-98	amphibolite	x									x		?	x	x			
46-100	amphibolite	x									x							
46-101	amphibolite	x									x				x			x
46-102	mica schist	x		x	x	x	x	x	x									
46-111	mica schist	x		x	x	x	x	x		x							x	x
46-112	amphibolite	x			x	x	x				x	?					x	
46-114	mica schist	x		x	x	x	x	x									x	x
46-115	amphibolite	x		x		?					x				x			
46-117	aplite	x		x	x		x				x		x	?				
46-118	pegmatite	x	x	x	x	x								x			x	
46-122	calcsilicate	?		x		x		x			x			x	x		x	
46-125	mica schist	x			x						x						x	
46-126	mica schist	x			x	x	x	x			*			?				
46-136	amphibolite	x		x	x						x				x		x	
46-139	pegmatite	x	x	x		x											x	
46-140	aplite	x	x	x		x											x	
46-149	calcsilicate	x		x				x			x		x	x	x		x	x
46-150	calcsilicate	x	x	x	x		?	x			x	x			x		x	
46-152	mica schist	x		x							x			?		x		
46-157	gneiss	x	x	x	x												x	x
46-158	quartzite	x	x	x	x													
46-161	mica schist	x		x	x	x	x	x	x							x	x	x
46-163	mica schist	x		x	x	x		x	x	?						x		x
46-165	amphibolite	x		x							x			x				
46-166	mica schist	x		x	x	x												
46-169	mica schist	x		x	x	x	x	x	x	x						x		
46-172	mica schist	x		x	x	x	x	x								x		x
46-173	mica schist	x		x	x	x	x	x								x		
46-174	mica schist	x		x	x	x	x	x										
46-175	mica schist	x		x	x	x	x	x	x									x
46-176	mica schist	x		x	x	x	x	x	x	x						x	x	x
46-180	mica schist	x		x	x	x											x	x
46-181	mica schist	x		x	x	x	x	x	x									x
46-182	mica schist	x		x	x	x	x	x	x							x	x	x
46-183	mica schist	x		x	x	x	x	x	x									x
46-184	mica schist	x		x	x	x	x	x	x									x

* cummingtonite rimmed with hornblende

Sample	Rock Type	Plagioclase	K-Feldspar	Quartz	Biotite	Muscovite	Chlorite	Garnet	Staurolite	Sillimanite	Hornblende	Actinolite	Calcite	Epidote	Sphene	Tourmaline	Apatite	Zircon
46-185	mica schist	x		x	x	x	x	x	x									x
46-188	aplite	x	x	x		x	x											
46-189	amphibolite	x		x			x				x			x	x			
46-190	aplite	x	x	x	x	x	x											
46-191	amphibolite	x									x				x			
46-192	amphibolite	x									x				x		x	
46-194	aplite	x		x	x		x											
46-195	aplite	x	x	x	x		x	x									x	
46-197	aplite	x	x	x	x	x	x											
46-198	aplite	x	x	x	x													
46-199	aplite (?)	x	x	x	x		x				x			?			x	
46-203	aplite	x	x	x	x	x	x											
46-205	amphibolite	x		x	x						x							
46-206	aplite	x	x	x	x	x	?										x	
46-207	aplite	x	?	x	x			x									x	
46-208	aplite	x	x	x	x	x	x	x										
46-209	aplite	x	x	x	x	x												